Insulin sensitivity and nutrient utilisation in skeletal muscle

by

Yan Yan Lam

Thesis submitted in fulfilment of the requirement for
the Degree of Doctor of Philosophy

Discipline of Medicine
School of Medicine
Faculty of Health Sciences
University of Adelaide, South Australia, Australia

November 2009

Chapter 1: Background

1.1 Introduction

Obesity is a condition in which fat accumulation in adipose tissue is in excess to an extent that health may be impaired. Obese individuals are at an increased risk of developing a range of chronic health problems including cardiovascular disease, type 2 diabetes, hypertension, non-alcoholic fatty liver disease and certain cancers (Reaven 2005). Insulin resistance is integral to the pathophysiology of obesity-related metabolic abnormalities (Eckel et al. 2005; Reaven 2005). Not all obese individuals are insulin-resistant and a subgroup, accounting for ~ 20% of the obese population, remains insulin-sensitive and maintains a normal metabolic profile (Karelis et al. 2004; Rasouli et al. 2007). It has been proposed that regional fat distribution and skeletal muscle mass and function determine insulin sensitivity and metabolic risk (Weiss 2007; Atlantis et al. 2009) and a low ratio of visceral fat to skeletal muscle is one of the key determinants of a favourable metabolic profile (Kim et al. 2004). A better understanding of the physiology, in particular the subtypes, of obesity and the specific pathways contributing to insulin resistance in obese individuals will be of significant importance for the development of effective strategies to prevent obesity-related complications. In this chapter, recent *in vivo* and *in vitro* data that implicate the regulation of insulin sensitivity, including the physiology of skeletal muscle and adipose tissue, as well as the crosstalk between the two tissue types will be reviewed.

1.2 Obesity and metabolic risk

Obesity is associated with numerous co-morbidities including cardiovascular disease, type 2 diabetes, some cancers, reproductive abnormalities and a significant reduction in

life expectancy (Haslam and James 2005). Not all obese individuals are at an increased metabolic and cardiovascular risk. A subset of obese individuals, classified as 'metabolically healthy obese', account for ~ 20% of the obese population; they remain insulin-sensitive and appear to be less susceptible to obesity-related metabolic complications (Rasouli et al. 2007). When compared to people with similar total body fat, metabolically healthy obese individuals have lower visceral fat content, a more favourable lipid profile including a higher circulating level of high density lipoprotein cholesterol and lower triglyceride, glucose and insulin (Karelis et al. 2004).

1.2.1 Intra-abdominal fat accumulation and insulin sensitivity

Fat deposition in the intra-abdominal depot as omental, mesenteric and retroperitoneal fat along the dorsal borderline of the intestines and the ventral surface of the kidney is referred to as central adiposity (Wajchenberg 2000). Epidemiological data suggest a relationship between central adiposity and metabolic risk factors including elevated blood pressure and fasting plasma glucose and triglycerides (Fox et al. 2007). In apparently healthy individuals (26 – 75 yr; BMI 18.4 – 46.8 kg/m^2), the intra-abdominal fat area was positively correlated with systolic and diastolic blood pressures, plasma glucose and triglycerides levels independent of insulin sensitivity (Carr et al. 2004). Visceral fat accounts for ~ 50% of the variance in insulin sensitivity (Kelley et al. 2000; Cnop et al. 2002) and has been shown to be a predictor for future insulin resistance (Hayashi et al. 2008). The accumulation of visceral fat is strongly related to decreased insulin sensitivity in both non-obese and obese individuals (Wajchenberg 2000; Karelis et al. 2004). Conversely, the association between visceral fat reduction and improved insulin sensitivity has been consistently demonstrated in obese (Lien et al. 2009), glucose

intolerance-impaired (Carr et al. 2005) and type 2 diabetic (Ibanez et al. 2005) individuals.

1.2.2 Subcutaneous fat accumulation and insulin sensitivity

In contrast to intra-abdominal fat, the relationship between abdominal subcutaneous adipose tissue and insulin sensitivity is equivocal. In a cohort of 174 lean insulin-sensitive, lean insulin-resistant and obese insulin-resistant individuals (42% male and 58% female), insulin sensitivity was inversely correlated with intra-abdominal ($P < 0.001$) but not abdominal subcutaneous ($P = 0.06$) fat and the two fat depots accounted for 54% and 5% of the variance in insulin sensitivity respectively. When only lean subjects were included in the analysis, insulin sensitivity was predicted by intra-abdominal but not abdominal subcutaneous fat (Cnop et al. 2002). In 1,457 Hispanic and African-American individuals (42% male and 58% female), both subcutaneous and visceral abdominal tissue were inversely correlated with insulin sensitivity irrespective of ethnicity, sex and obesity status. In addition, there is an interaction between the two fat depots such that when both fat areas are high, insulin sensitivity is extremely low (Wagenknecht et al. 2003).

The differential metabolic effects of subdivisions of abdominal subcutaneous fat may account for the variations of the fat depot on insulin sensitivity documented in the literature. Traditionally regarded as a homogenous compartment, the abdominal subcutaneous tissue is separated by a stromal fascia into histologically and functionally distinct superficial (sSAT) and deep subcutaneous adipose tissue (dSAT) (Walker et al. 2007). Independent of the obesity status, sSAT accounts for ~ 40% and ~ 30% of cross-sectional abdominal adipose tissue in women and men respectively whereas both gender

have similar (~ 35%) dSAT (Kelley et al. 2000). While neither thigh adipose tissue nor sSAT has any effect, dSAT is negatively correlated with insulin-stimulated glucose metabolism and the relationship is independent of total body fat and visceral fat. In addition, the combination of dSAT and visceral fat has a stronger negative correlation with insulin sensitivity compared to the effect of either fat depot (Kelley et al. 2000). *In vitro*, a decrease in the protein content of leptin, an adipokine known to improve insulin sensitivity (Section 1.4.3.1) was observed in adipocytes isolated from sSAT to dSAT through to visceral fat. Conversely, adipocytes from dSAT and visceral fat had higher mRNA and protein content of resistin, an adipokine which may induce insulin resistance (Section 1.5.3.6) (Walker et al. 2007). Taken together, these data suggest that the sSAT and dSAT are metabolically distinct fat depots and the latter has a transcript and protein expression profile similar to visceral fat, which may contribute to the relationship between abdominal subcutaneous fat and insulin sensitivity. In addition, it has been proposed that once the accumulation of visceral adipose tissue exceeds a certain threshold, the contribution of the depot to insulin resistance would overwhelm that of abdominal subcutaneous fat regardless of subdivisions (Ross et al. 2002).

1.2.3 Factors influencing regional adiposity

The distribution of adipose tissue varies considerably among individuals even with similar total body fat. Gender, age and ethnicity have been shown to affect regional adiposity. Men tend to store more visceral fat and have at least twice the proportion of fat localised to the intra-abdominal depot as compared to women (Bjorntorp 1990; Wajchenberg 2000). The gender-specific difference in fat distribution appears to diminish in older ages as females tend to develop central adiposity after menopause (Ito et al. 2001). Ethnicity also affects regional adiposity. Aboriginal men and women in

Australia have been shown to have greater waist-to-hip ratio (WHR) as compared to their European Australian counterparts and the difference is observed across all BMI levels up to 30 kg/m^2 (Piers et al. 2003). Central obesity is also more common in Hispanic as compared to white women in early adulthood (Casas et al. 2001).

Gender (Lindle et al. 1997), age (Frontera et al. 2008) and ethnicity (Newman et al. 2003) concomitantly affect skeletal muscle mass and strength, suggesting a possible link between skeletal muscle function and regional adiposity. Indeed, a negative relationship between lean body mass and visceral fat has been observed in sedentary obese post-menopausal women (Brochu et al. 2001). In addition, skeletal muscle mass and/or strength together with regional adiposity have been shown to be associated with insulin sensitivity. In a cohort of well-functioning and non-diabetic adults (70 – 79 yr), decreased quadriceps muscle mass and strength/kg muscle mass was associated with insulin resistance (Barzilay et al. 2009). A high visceral fat-to-skeletal muscle ratio is also negatively correlated with insulin sensitivity in overweight women (49.7 ± 5.3 yr; BMI 26.1 ± 2.5 kg/m^2) (Kim et al. 2004). Taken together, these data suggest that the interaction between skeletal muscle and adipose tissue is important in the regulation of insulin sensitivity and possibly critical in the development of obesity-related metabolic complications.

1.3 Energy metabolism in skeletal muscle

In healthy lean humans, skeletal muscle accounts for 40 – 45% of total body mass and is a major determinant of resting energy expenditure, accounting for 40 – 50% of the variability in basal metabolic rate and up to 75% of glucose disposal (Zurlo et al. 1990; Lopez-Soriano et al. 2006). The capacity for skeletal muscle to utilise either fatty acid or

glucose as an energy substrate and the effectiveness of alternating between the two fuels is essential to maintain whole-body energy homeostasis under a wide range of physiological conditions (de Beaudrap et al. 2006). Individuals with a reduced energy expenditure as a consequence of lower resting metabolism in skeletal muscle are at greater risk for sustained positive energy balance and therefore weight gain (Zurlo et al. 1990). The regulation of oxidative capacity and the physiology of glucose and fatty acid metabolism in skeletal muscle, as well as their relationship with obesity and insulin resistance is described below.

1.3.1 Oxidative capacity of skeletal muscle

1.3.1.1 Muscle oxidative capacity is dependent on fibre type composition

Skeletal muscle is composed of fibres with unique contractile and metabolic characteristics. Based on the expression of various isoforms of myosin heavy chains and myosin light chains, the fibres in mammalian skeletal muscle are broadly classified into three types, namely types I, IIa and IIb (Schiaffino and Reggiani 1994). Slow-twitch type I fibres have the highest oxidative capacity, followed in order by fast-twitch oxidative type IIa and fast-twitch glycolytic IIb (Kelley 2002). The fibre type-specific oxidative capacity is concomitant with the relative abundance of mitochondria, with the highest mitochondrial density in the type I fibres and the lowest in type II fibres (Berchtold et al. 2000). In addition, the capacity of mitochondria to utilise energy substrates is fibre type-specific. Mitochondria from type I fibres have been shown to have similar capacity to oxidise fatty acid and glucose, whereas the capacity of type II fibres to oxidise fatty acid is ~ 40% lower as compared to glucose (Mogensen and Sahlin 2005).

The abundance of mitochondria is mainly regulated by peroxisome proliferator-activated receptor-γ coactivator (PGC)-1α, a transcription factor that increases the transcription of a range of mitochondrial genes including β-ATP synthase, cytochrome-c, cytochrome-c-oxidase subunit IV and mitochondrial transcription factor A and subsequently promotes mitochondrial biosynthesis (Puigserver and Spiegelman 2003). PGC-1α expression is modified according to energy demand, which in turn leads to fibre type conversion and changes in oxidative capacity of skeletal muscle.

1.3.1.2 Reduced muscle oxidative capacity in obesity

Obesity is associated with a lower oxidative capacity and an altered fibre type composition in skeletal muscle. For example it has been shown that in obese individuals body fat is negatively correlated with the percentage of type I fibres and positively correlated with type II fibres (Kriketos et al. 1996).

Traditionally the reduction in muscle oxidative capacity in obesity is thought to be a consequence of mitochondrial dysfunction and/or deficiency, a concept that has recently been challenged. Mitochondria isolated from lean and obese individuals have similar capacity to oxidise fatty acids, arguing against a specific functional defect in the mitochondria of obese individuals (Holloway et al. 2009). The reduced rates of whole-muscle oxidative capacity are rather the consequence of lower mitochondrial abundance. Despite having ~ 30% less mitochondria in their muscles, type 2 diabetic, obese and insulin-resistant individuals have normal aerobic metabolism under free-living conditions and the capacity to oxidise fatty acids remains in excess in relation to requirements in the resting state (Kraegen et al. 2008; Holloszy 2009). Taken together, these data suggest that the oxidative capacity of skeletal muscle in obese individuals is reduced if not

significantly impaired; nevertheless they are more susceptible to the effects of nutrient overload.

1.3.2 Skeletal muscle glucose metabolism

1.3.2.1 Glucose transport

Glucose, which is hydrophilic, enters the cytoplasm by a process of facilitated transport. To date, 13 isoforms of facilitated glucose transporters (GLUTs) have been identified. These vary in their maximal rates of glucose transport and sensitivity to hormonal regulation (Bouche et al. 2004). GLUT1 and GLUT4 are the main glucose transporters in skeletal muscle (Zorzano et al. 2000). GLUT1 is predominantly responsible for glucose transport under basal conditions, and its activity is increased by metabolic stress via the activation of adenosine monophosphate (AMP)-activated protein kinase (AMPK) (Section 1.3.4.3) (Bouche et al. 2004). GLUT4 mediates the effect of insulin on promoting glucose uptake in skeletal muscle (Larance et al. 2008), a process that accounts for ~ 75% of whole-body insulin-stimulated glucose uptake (Corcoran et al. 2007).

The molecular mechanisms by which insulin-stimulated glucose uptake occurs are detailed in reviews by Khan and Pessin (2002) and Watson and Pessin (2001) and are summarised in Figure 1.1. Briefly, insulin binds to its receptor at the plasma membrane and autophosphorylation of the receptor occurs. The activation of insulin receptor facilitates the binding and the subsequent tyrosine phosphorylation of the insulin receptor substrate (IRS) family of proteins. IRS-1, and to a lesser extent IRS-2, recruit and activate phosphatidylinositol 3-kinase (PI3K), which generates phosphatidylinositol(3,4,5)-trisphosphate (PIP3) and subsequently activates 3-

phosphoinositide-dependent protein kinase (PDPK)-1. PDPK1 phosphorylates and activates other kinases including atypical protein kinase C (aPKC) and Akt, which stimulate GLUT4 vesicle exocytosis. Finally, the translocation and fusion of the GLUT4 storage vesicles with the plasma membrane increases glucose uptake into the skeletal muscle cells.

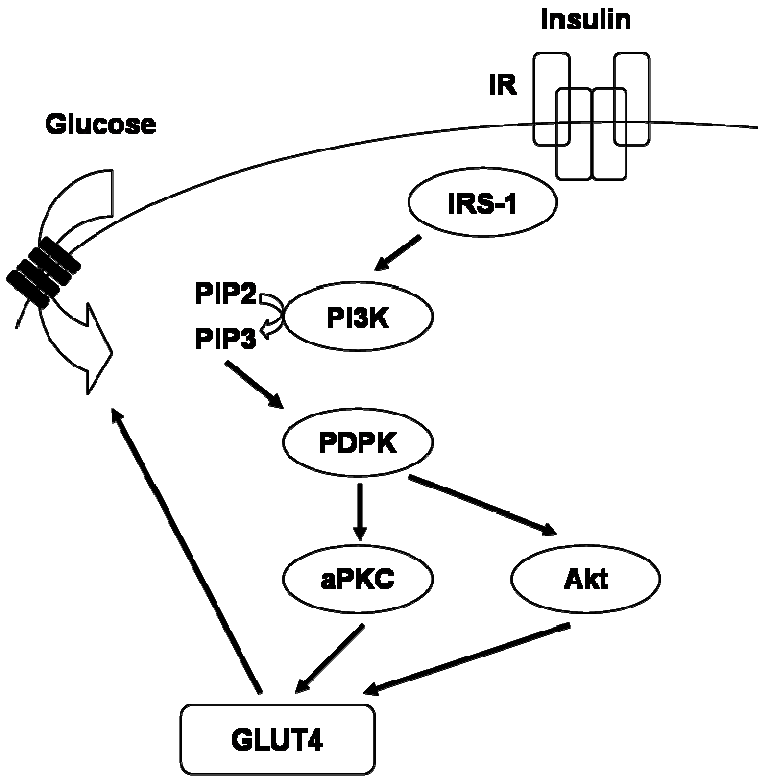

Figure 1.1. Schematic model for insulin-stimulated GLUT4 translocation in skeletal muscle. The binding of insulin to its receptor (IR) on the plasma membrane activates insulin receptor substrate (IRS)-1. IRS-1 activates phosphatidylinositol 3-kinase (PI3K) to generate phosphatidylinositol(3,4,5)-trisphosphate (PIP3) from phosphatidylinositol(4,5)-bisphosphate (PIP2), which stimulates the activity of 3-phosphoinositide-dependent protein kinase (PDPK)-1. Finally, the activated atypical protein kinase C (aPKC) and Akt promote GLUT4 translocation from intracellular compartments to the plasma membrane.

1.3.2.2 Glucose utilisation

Once transported into the cytoplasm, glucose is rapidly phosphorylated to glucose-6-phosphate (G-6-P) to maintain a concentration gradient for glucose uptake, a process catalysed mainly by hexokinase II in skeletal muscle (Bouche et al. 2004). Subsequently, glucose either enters glycolysis for oxidation or biosynthetic pathways to generate glycogen and hexosamine.

Glycolysis is the first step by which glucose is oxidised to release energy (Figure 1.2). Each G-6-P is converted to two pyruvate molecules which, when under aerobic conditions, are transported into the mitochondria and converted to acetyl-coenzyme A (CoA) by the pyruvate dehydrogenase complex (PDC). Finally, acetyl-CoA enters the tricarboxylic acid (TCA) cycle, where it is oxidised to carbon dioxide to release energy (Bouche et al. 2004). PDC activity is a major point of regulation for glucose oxidation and is in turn regulated by a reversible phosphorylation/dephosphorylation cycle – specifically pyruvate dehydrogenase kinase (PDK) inhibits PDC by phosphorylation and the effect is reversed by dephosphorylation catalysed by pyruvate dehydrogenase phosphatase (PDP) (Abbot et al. 2005). Among the four isoforms of PDK genes (PDK1 – 4) identified in humans, PDK2 and PDK4 are the most abundant in skeletal muscle and the later is highly sensitive to changes in diet and exercise. High-fat feeding for 3 days increased PDK activity, PDK4 mRNA and protein content in the skeletal muscle of healthy young men (Peters et al. 2001). Similarly, a 5-day exercise training protocol and a single prolonged cycling bout increased skeletal muscle PDK4 mRNA content by 4- to 6-fold and > 20-fold respectively during the subsequent 2 h of recovery in healthy male subjects (Pilegaard et al. 2000).

Glucose transported into skeletal muscle may also enter one or more biosynthetic pathways. Glycogenesis is a process by which glucose is converted to glycogen to provide energy for muscle contraction and accounts for the majority of insulin-stimulated glucose uptake in skeletal muscle (Bouche et al. 2004). Glycogen synthase is the rate-limiting enzyme in glycogenesis and is up-regulated by insulin. Insulin-activated Akt inhibits glycogen synthase kinase-3 by phosphorylation and subsequently increases glycogen synthase activity (Bouche et al. 2004).

A small amount (~ 1 – 3%) of glucose in skeletal muscle enters the hexosamine biosynthetic pathway, a process by which substrates are generated for glycoprotein synthesis (Hawkins et al. 1997).

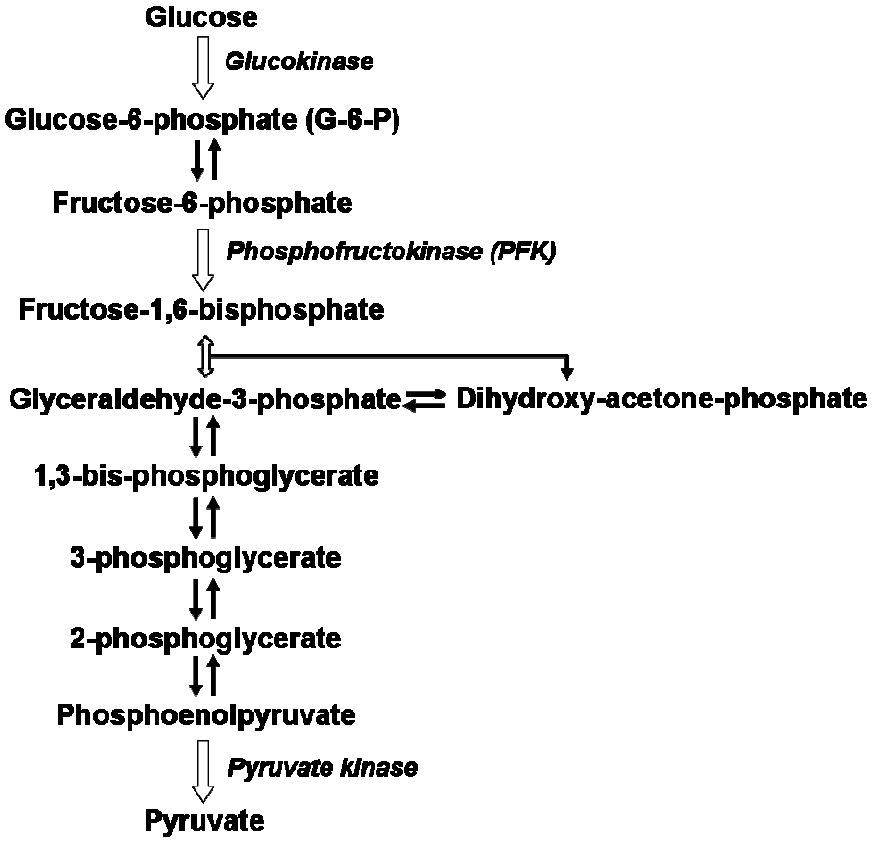

Figure 1.2. Glycolysis in skeletal muscle. Once transported into the cytoplasm, glucose is phosphorylated to form glucose-6-phosphate and in turn fructose-6-phosphate. The subsequent phosphorylation of fructose-6-phosphate by phosphofructokinase forms fructose-1,6-bisphosphate, which after sequential conversions forms phosphoenolpyruvate. Finally, pyruvate kinase catalyses the formation of pyruvate.

1.3.3 Skeletal muscle fatty acid metabolism

1.3.3.1 Fatty acid transport

Because skeletal muscle has a limited capacity to store lipids, the membrane transport of long-chain fatty acids is tightly regulated to prevent intramuscular lipid accumulation. Fatty acid transport in skeletal muscle is regulated at the plasma and mitochondrial membranes via both common and distinct mechanisms.

Fatty acid uptake into the cytoplasm

The uptake of long-chain fatty acids across the plasma membrane is regulated by the expression and/or activity of carrier proteins including fatty acid translocase (FAT/CD36), plasma membrane fatty acid-binding protein (FABPpm) and fatty acid transport proteins (FATPs) (Jeukendrup 2002). Diet and exercise are known regulators of fatty acid carrier proteins. A 5-day intervention of a high-fat diet (> 65% of energy as lipids) increased the mRNA and protein content of FAT/CD36 in skeletal muscle of healthy humans by ~ 50% and ~ 25% respectively (Cameron-Smith et al. 2003). Similarly, 3 weeks of intense one-legged endurance training increased FABPpm protein content in skeletal muscle by 49% and the effect was localised only to the muscle engaged in the training (Kiens et al. 1997). These data demonstrate the adaptive capacity of the skeletal muscle to utilise the predominant energy substrate and provide evidence for the functional significance of the fatty acid transport mechanisms.

Fatty acid uptake into the mitochondria

The transport of long-chain fatty acids into the mitochondria is generally considered as the rate-limiting step in fatty acid oxidation (Jeukendrup 2002). The process of

mitochondrial fatty acid uptake is detailed in a review by Jeukendrup (2002) and is summarised in Figure 1.3. Carnitine palmitoyltransferase (CPT)-I, located on the outer mitochondrial membrane, facilitates the binding of carnitine to long-chain acyl-CoA. The resulting acyl-carnitine complex is then transported across the mitochondrial membrane by carnitine-acylcarnitine translocase (CACT) and subsequently acyl-CoA is regenerated at the matrix side of the inner mitochondrial membrane by CPT-II.

The capacity of the CPT system to transport fatty acids across the mitochondrial membrane depends largely on the activity of CPT-I, which is regulated by an allosteric inhibitor malonyl-CoA. Acetyl-CoA carboxylase (ACC) catalyses the carboxylation of cytosolic acetyl-CoA to form malonyl-CoA. Under resting conditions, intramuscular concentration of malonyl-CoA is sufficiently high to inhibit CPT-I activity (Jeukendrup 2002). When ACC is inhibited by phosphorylation, the reduction in malonyl-CoA synthesis releases the inhibition of CPT-I and the transport of long-chain fatty acids into the mitochondria increases (Brownsey et al. 2006). Conversely, allosteric modulators including citrate, an intermediate from the TCA cycle, activate ACC and the subsequent inhibition of CPT-I reduces substrate availability for fatty acid oxidation to prevent excessive ATP production (Brownsey et al. 2006).

Recent studies revealed that mitochondrial fatty acid uptake is also mediated by fatty acid carrier proteins. FAT/CD36 is identified in mitochondria isolated from human skeletal muscle and an inverse relationship has been demonstrated between FAT/CD36 inhibition and fatty acid oxidation (Bezaire et al. 2006). Over-expressing

FATP1 in isolated mitochondria in L6E9 rat skeletal muscle cells increased fatty acid oxidation and the effect was additive to that of over-expressing CPT-I (Sebastian et al. 2009). It has been proposed that these fatty acid carrier proteins work in conjunction with CPT-I and may be important under conditions in which there is an increased demand for fatty acid oxidation including during exercise or muscle contraction (Sebastian et al. 2009).

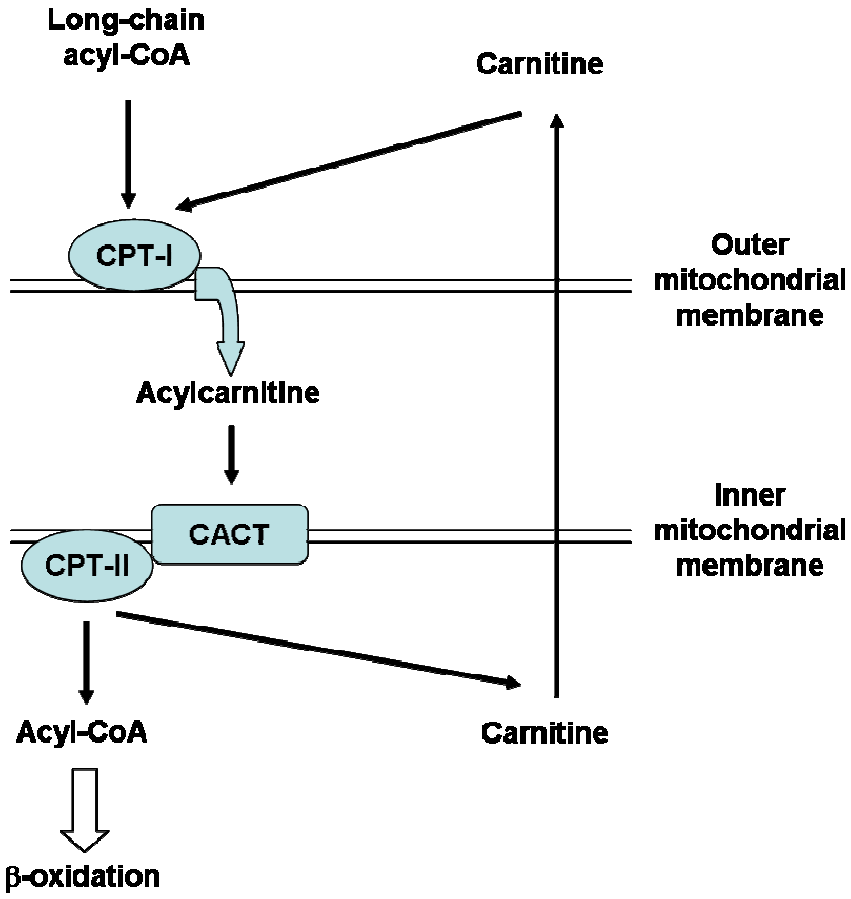

Figure 1.3. The transport of long-chain fatty acids into the mitochondria via the carnitine palmitoyltransferase (CPT) system. CPT-I catalyses the binding of long-chain acyl-CoA to carnitine. Carnitine-acylcarnitine translocase (CACT) transports the acylcarnitine complex to the mitochondrial inner membrane. At the matrix side of the inner mitochondrial membrane, CPT-II regenerates acyl-CoA which then undergoes β-oxidation. Carnitine is released and diffuses into the cytoplasm.

Abnormalities of fatty acid transport in obesity and insulin resistance

Obesity and insulin resistance are characterised by dysregulation of both cytoplasmic and mitochondrial fatty acid uptake in the skeletal muscle. In obese and type 2 diabetic individuals, fatty acid transport into the cytoplasm is up-regulated, which is a consequence of impaired translocation of fatty acid carrier proteins (Bonen et al. 2004). The high basal expression of the fatty acid carrier proteins at the plasma membrane promotes fatty acid uptake into the cytoplasm (Bandyopadhyay et al. 2006) and is inversely related to insulin sensitivity (Fisher and Gertow 2005). Conversely, mitochondrial fatty acid uptake in skeletal muscle is reduced in obese individuals, an observation associated with a ~ 35% lower CPT-I activity as compared to healthy controls (Kim et al. 2000). In skeletal muscle of insulin-resistant subjects, the high basal activity of ACC leads to increased intramuscular malonyl-CoA content, which subsequently inhibits CPT-I activity (Bandyopadhyay et al. 2006). Taken together, the combined effect of an increased fatty acid uptake into the cytoplasm and a reduced transport into the mitochondria leads to an accumulation of fatty acids in skeletal muscle of obese and/or insulin resistant individuals.

1.3.3.2 Fatty acid utilisation

Once transported into the skeletal muscle cells, fatty acids enter the mitochondria for oxidation, or they are incorporated into various lipids including phospholipids to maintain cellular structural integrity, triglycerides for storage, or accumulate as intramuscular lipid metabolites such as diacylglycerol (DAG) and ceramide. The partition of fatty acids towards various metabolic pathways depends on energy demand as well as substrate specificity, expression and activity of particular enzymes involved in the metabolic pathways.

Fatty acid oxidation

Skeletal muscle is the main site for fatty acid oxidation. When fatty acids are transported into the mitochondria, they undergo β-oxidation, a process by which the fatty acid chains are broken down into acetyl-CoAs, and subsequently enter the TCA cycle (Jeukendrup 2002). Under resting conditions, fatty acids are the substrate predominantly used for energy in skeletal muscle (Jeukendrup 2002). It has been shown that fatty acid oxidation in skeletal muscle of obese individuals and type 2 diabetic patients was ~ 50% and ~ 30% lower respectively when compared to healthy controls (Kim et al. 2000; Bandyopadhyay et al. 2006). In addition, the resting fatty acid oxidation in skeletal muscle is inversely correlated with BMI up to 30 kg/m^2, beyond which the reduction in fatty acid oxidation seems to plateau (Kim et al. 2000).

Incorporation into tissue lipids

After uptake into skeletal muscle, ~ 60 – 90% of fatty acids are incorporated into phospholipids and ~ 5 – 40% into triglycerides (Montell et al. 2001). Fatty acid composition of phospholipids in skeletal muscle reflects the fatty acid profile of the diet (Vessby et al. 2002). In healthy humans, whole-body insulin sensitivity is positively correlated with the abundance of long-chain polyunsaturated (Borkman et al. 1993) and negatively with saturated fatty acids (Vessby et al. 1994) in the skeletal muscle phospholipids. The relationship between fatty acid composition of the phospholipids and insulin sensitivity in the skeletal muscle will be detailed in Section 1.5.

In skeletal muscle, triglycerides are stored as lipid droplets which serve as an energy supply, a reserve depot for lipid precursors, and as a buffer from sudden influxes of fatty acids and acyl-CoAs (Coleman and Lee 2004). The incorporation of fatty acids into intramuscular triglyceride stores involves multiple biochemical pathways. The rate-limiting enzymes include glycerol kinase, 1-acylglycerol-3-phosphate acyltransferase (AGPAT)-α and diacylglyceroltransferase (DGAT)-1 (Agarwal and Garg 2003; Coleman and Lee 2004; Moro et al. 2008) (Figure 1.4). Briefly, glycerol kinase converts glycerol to glycerol-3-phosphate, which then undergoes a series of acylation by glycerol-3-phosphate acyltransferase and AGPAT-α to form phosphatidic acid, which is subsequently converted to DAG. Finally, DAG is acylated by DGAT to produce triglyceride.

In non-diabetic male Pima Indians, triglyceride content in skeletal muscle is associated with insulin resistance, an observation independent of measures of obesity including percentage of body fat, BMI and waist-to-thigh ratio (Pan et al. 1997). Compared to healthy controls, obese non-diabetic and obese-diabetic patients have ~ 80% and ~ 150% higher intramuscular triglyceride respectively (Goodpaster et al. 2000). There is an inverse relationship between intramuscular triglyceride content and insulin sensitivity (Goodpaster and Wolf 2004). Triglyceride by itself, however, does not appear to be a direct cause for insulin resistance. Endurance-trained athletes have been shown to have ~ 60% higher intramuscular lipid compared to lean sedentary subjects and yet both groups are equally insulin-sensitive (Goodpaster et al. 2001). It has been proposed that intramuscular triglyceride content may be a surrogate marker for other lipid species in muscle which induce insulin resistance (Goodpaster and Kelley 2002).

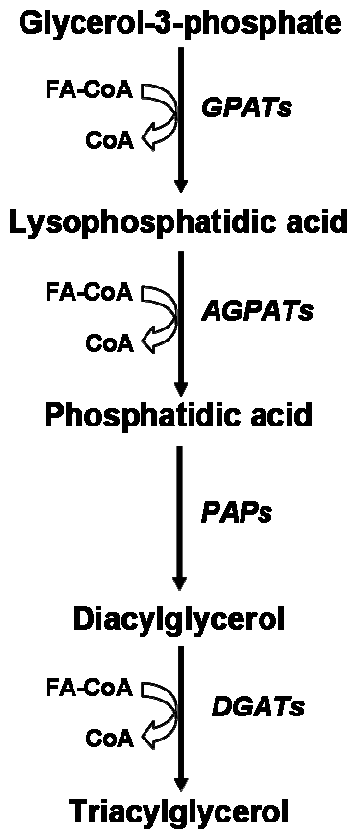

Figure 1.4. Triglyceride synthesis in skeletal muscle. Glycerol-3-phosphate undergoes sequential acylation by glycerol-3-phosphate acyltransferase (GPAT) and 1-acylglycerol-3-phosphate acyltransferase (AGPAT) to form phosphatidic acid. The phosphate group is then removed by phosphatidate phosphohydrolase (PAP) to produce diacylglycerol (DAG). Finally, DAG is further acylated by diacylglycerol acyltransferase (DGAT) to form triacylglycerol.

Accumulation of DAG and ceramide

DAG in skeletal muscle is mainly derived from *de novo* synthesis as part of triglyceride formation, and to a lesser extent from the breakdown of phospholipids and phosphatidycholine (Timmers et al. 2008). In obese individuals, the elevated DAG content in skeletal muscle is associated with decreased insulin sensitivity (Straczkowski et al. 2007). In rats, high-fat feeding increases DAG content and reduces insulin-stimulated glucose uptake in skeletal muscle (Todd et al. 2007). Similarly, in humans a lipid load delivered intravenously over 6 h reduces whole-body insulin sensitivity in healthy humans, an effect associated with an elevated DAG content in skeletal muscle (Itani et al. 2002). The inhibitory effect of DAG on insulin signal transduction is thought to be mediated by the inflammatory pathways (Section 5.1). Briefly, the activation of DAG-sensitive novel protein kinase C (nPKC) up-regulates the nuclear factor kappa B (NFκB) signalling pathway and subsequently leads to serine phosphorylation of IRS-1 (Holden et al. 2008; Lee et al. 2008).

Ceramide, a precursor of complex sphingolipids, modulates cellular functions including proliferation, differentiation and apoptosis (Hanada 2003). In skeletal muscle, ceramide is predominantly generated from *de novo* synthesis and to a lesser extent from hydrolysis of plasma membrane sphingomyelin (Straczkowski and Kowalska 2008). Serine palmitoyltransferase (SPT) catalyses the condensation of palmitoyl-CoA and serine to form 3-keto-sphinganine, a rate-limiting step in sphingolipid synthesis, which leads to the sequential synthesis of sphinganine, dihydroceramide and ceramide (Summers 2006) (Figure 1.5). SPTLC1 and SPTLC2 encode the regulatory and the catalytic subunits of SPT respectively (Hanada 2003).

Obese individuals have increased ceramide accumulation in skeletal muscle and the intramuscular ceramide content is inversely related to insulin sensitivity (Straczkowski et al. 2007). High-fat diet in rats (Lee et al. 2006) and lipid infusion in healthy humans (Straczkowski et al. 2004) both have been shown to induce an increase in intramuscular ceramide content, an effect associated with decreased whole-body insulin sensitivity. A ceramide analogue (C_2-ceramide) reduces insulin-stimulated glucose uptake in a dose-dependent manner in L6 myotubes (Hajduch et al. 2001).

Ceramide-induced insulin resistance involves the attenuation of Akt activation and/or acceleration of Akt dephosphorylation. In L6 myotubes, PA induced an increase in PKC-ζ activity which impaired the insulin-stimulated binding of Akt to PIP3, an effect prevented by a specific SPT inhibitor myriocin (Powell et al. 2004). Inhibiting protein phosphatase (PP)-2A, an enzyme that desensitises the effect of insulin on Akt activation by accelerating Akt dephosphorylation, also abolished the effect of ceramide on inhibiting insulin-stimulated Akt activation in C2C12 myotubes (Chavez et al. 2003).

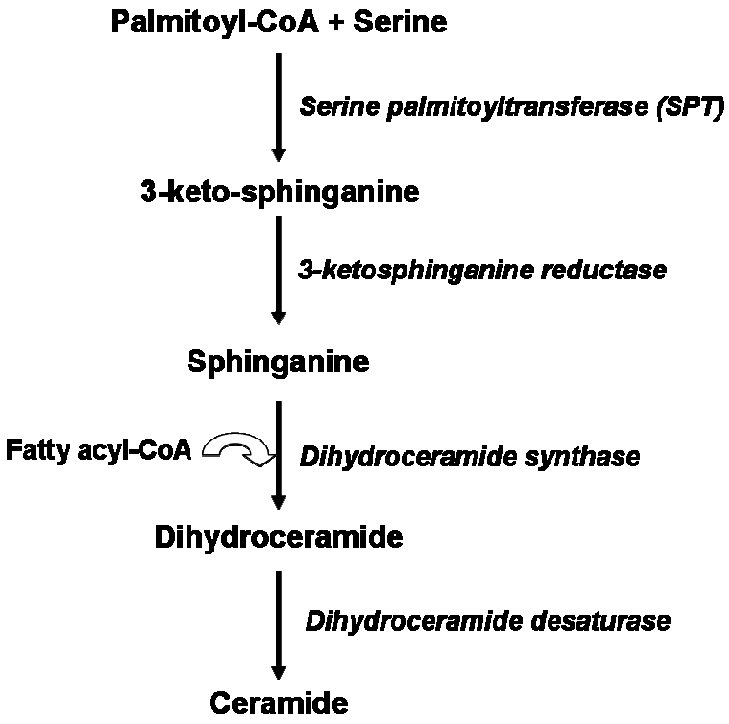

Figure 1.5. ***De novo*** **synthesis of ceramide in skeletal muscle.** Serine palmitoyltransferase (SPT) catalyses the condensation of palmitoyl-coenzyme A (CoA) and serine. Ketosphinganine then undergoes reduction to form sphinganine, which is subsequently acylated to produce dihydroceramide. Finally, a desaturase catalyses the formation of a trans 4,5-double bond to produce ceramide.

1.3.4 Metabolic flexibility of skeletal muscle

The availability of substrates is a major determinant in energy metabolism in skeletal muscle. The efficient transition between utilising fatty acids and glucose allows skeletal muscle to adapt to the intensity of metabolic demands and substrate availability (de Beaudrap et al. 2006). In healthy individuals, fatty acid oxidation in skeletal muscle increases with increasing exercise intensity until reaching ~ 65% maximal oxygen consumption, after which fatty acid oxidation is reduced (Jeukendrup 2002). In contrast, glucose oxidation increases as a function of the aerobic rate and utilising glucose for energy is the only option under anaerobic conditions (Jeukendrup 2002; Whipp 2007).

The ability of skeletal muscle to switch from using predominately fatty acids during fasting conditions to increase glucose uptake, oxidation and storage in response to insulin, and at the same time suppressing fatty acid oxidation, is known as 'metabolic flexibility' (Kelley and Mandarino 2000). Immediately after a 3 h lipid infusion, a glucose flux induced by a 5 h hyperglycaemic/hyperinsulinaemic clamp reduced whole-body fatty acid oxidation (Sidossis and Wolfe 1996). In primary human myotubes derived from healthy individuals, extracellular glucose concentration is positively related to the suppression of fatty acid oxidation (Ukropcova et al. 2005). Metabolic flexibility, defined as the change in respiratory quotient during an euglycaemic-hyperinsulinaemic clamp, is positively correlated with insulin sensitivity and inversely correlated with percentage of body fat (Ukropcova et al. 2005).

1.3.4.1 Mechanisms of energy substrate transition

The Randle cycle describes a molecular mechanism by which the transition between oxidative fuels occurs (Figure 1.6). According to the Randle cycle (Randle et al. 1963),

an increase in plasma levels of fatty acids promotes fatty acid uptake into the skeletal muscle. The fatty acids enter β-oxidation to generate acetyl-CoA, which inhibits the activity of PDH to reduce the transport of pyruvate into the mitochondria for oxidation. In addition, citrate generated from oxidising fatty acids in the TCA cycle inhibits the activity of PFK (Figure 1.2). The subsequent accumulation of G-6-P inhibits hexokinase II and reduces glucose uptake into the skeletal muscle (Jequier 1998). Conversely, under conditions of high glucose availability, glucose oxidation increases the cytosolic concentration of citrate, an allosteric activator of ACC, and in turn increases intramuscular malonyl-CoA (Saha et al. 1997). The subsequent allosteric inhibition of CPT-I reduces the uptake of fatty acids into the mitochondria and therefore reduces fatty acid oxidation (Kelley and Mandarino 2000).

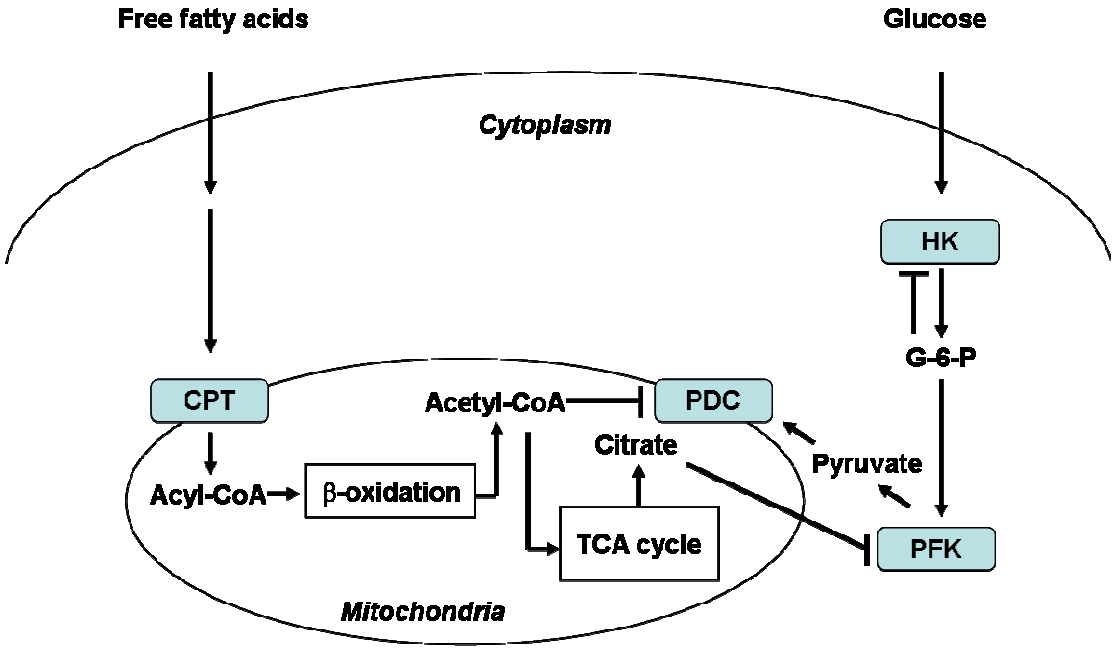

Figure 1.6. The Randle cycle. After uptake into the cytoplasm, fatty acids are transported into the mitochondria by the carnitine palmitoyltransferase (CPT) system. The fatty acids undergo β-oxidation to generate acetyl-coenzyme A (CoA) which then enters the tricarboxylic acid (TCA) cycle. Accumulation of acetyl-CoA and citrate inhibits the pyruvate dehydrogenase complex (PDC) and phosphofructokinase (PFK) respectively. The subsequent intracellular increase in glucose-6-phosphate (G-6-P) content inhibits hexokinase (HK) and finally reduces glucose uptake.

1.3.4.2 Metabolic inflexibility in obesity and insulin resistance

Insulin resistance is characterised by 'metabolic inflexibility', a situation in which substrate partitioning in fasting and insulin-stimulated conditions in skeletal muscle is impaired (Ukropcova et al. 2005; de Beaudrap et al. 2006). In obese insulin-resistant and type 2 diabetic patients, the transition from a predominant reliance on fatty acid oxidation during fasting to predominantly glucose oxidation in response to insulin is reduced in skeletal muscle. Metabolic inflexibility has been demonstrated in a study by Kelley et al (1999). In healthy controls, fatty acid oxidation accounted for ~ 60% of energy expenditure in skeletal muscle, which was reduced to ~ 10% in response to insulin infusion. In contrast, fatty acid oxidation in obese insulin-resistant individual contributed to ~ 40% of energy expenditure and was unaffected by insulin.

To date the molecular mechanisms by which metabolic inflexibility occurs remain unclear. Based on the fairly consistent absolute rate of fatty acid oxidation in obese individuals irrespective of physiological conditions, Kelley (2005) proposed that metabolic inflexibility is a consequence of an impaired regulation of fatty acid oxidation in skeletal muscle, which may lead to lipid-induced insulin resistance and subsequently modifies glucose metabolism. In contrast, Galgani et al (2008) suggest that metabolic flexibility is a consequence of insulin resistance, which reduces glucose uptake. The decreased availability of glucose for oxidation therefore leads to reliance on fatty acid oxidation to release energy. *In vivo*, metabolic flexibility also depends on the availability of nutrients to skeletal muscle, for example the capacity of adipose tissue to store and release free fatty acids (Galgani et al. 2008).

1.3.4.3 The role of AMPK in metabolic flexibility

AMPK is an important mediator of energy substrate transition in skeletal muscle. The structure, physiological role and regulation of AMPK are detailed in recent reviews by Long and Zierath (2008) and Towler and Hardie (2007). Briefly, AMPK is a heterotrimeric complex composed of a catalytic α- and regulatory β- and γ-subunits. There are two isoforms of the α-subunit, α1 is predominant in the cytoplasm and α2 in the nucleus, and both have similar substrate specificities. AMPK is a sensor of cellular energy status. An increased ratio of cellular AMP/ATP concentration, as in the case of ATP depletion, activates AMPK which subsequently up-regulates the ATP-generating pathways. In skeletal muscle, AMPK is mainly activated by its upstream kinase LKB1.

The activity of AMPK in skeletal muscle varies in response to energy status and substrate availability. In skeletal muscle of healthy humans, AMPKα2 activity increases with exercise intensity (Chen et al. 2003) and when glycogen has been depleted (Wojtaszewski et al. 2003). In contrast, AMPKα1 activity is only modestly increased during medium exercise intensity and remains relatively unchanged irrespective of further increase in exercise intensity (Chen et al. 2003). Substrate availability also affects AMPK activation. A high-fat diet increased whole-body fatty acid oxidation, an effect associated with elevated activity of both AMPKα1 and α2 in human skeletal muscle (Yeo et al. 2008). Conversely, glucose infusion reduced AMPKα2 activity in rat oxidative skeletal muscle (Kraegen et al. 2006). The direct effect of AMPK on energy substrate transition has been demonstrated using a specific AMPK activator 5-aminoimidazole-4-carboxamide-1-β-D-ribofuranoside (AICAR). Incubating skeletal muscle isolated from fed rats with AICAR increased fatty acid oxidation and reduced glucose oxidation but had no effect on glucose uptake (Kaushik et al. 2001). Taken together, these data suggest

that AMPK promotes fatty acid oxidation in skeletal muscle. Accordingly, AMPK activity is important in up-regulating energy metabolism according to energy demands and determines the relative utilisation of fatty acids and glucose to release energy during fasting/fed states.

AMPK increases fatty acid oxidation by up-regulating both fatty acid transport and oxidative function of mitochondria. The regulation of fatty acid oxidation in skeletal muscle by AMPK is detailed in reviews by Osler and Zierath (2008) and Long and Zierath (2008). Briefly, AMPK phosphorylates and thus inactivates ACC. The subsequent reduction in intramuscular malonyl-CoA content releases the inhibition on CPT-I and promotes fatty acid uptake into the mitochondria. The effect of AMPK on increasing fatty acid oxidation is also mediated by a concomitant increase in the expression of genes regulating muscle energy metabolism. One of the main transcriptional effectors of the AMPK pathway is peroxisome-proliferator-activated receptor (PPAR)-α. PPAR-α increases the expression of genes involved in fatty acid uptake, peroxisomal and mitochondrial β-oxidation including ACO, CPT1 and FABP3 to promote fatty acid oxidation (Lafontan and Viguerie 2006). In addition, AMPK has also been shown to increase the expression and activity of PGC-1α, which induces mitochondrial biogenesis and therefore further enhances the oxidative capacity of skeletal muscle (Jager et al. 2007).

Despite normal protein expression and AMPK activity (Hojlund et al. 2004), skeletal muscle of obese and type 2 diabetic individuals are less responsive to exercise-induced increase in AMPKα2 activity (Sriwijitkamol et al. 2007). While the molecular mechanisms by which the attenuated exercise-induced AMPK activation in obesity and

insulin resistance remain unclear (Sriwijitkamol et al. 2007), other factors affecting skeletal muscle metabolism including cytokines from adipose tissue and circulating fatty acids may also alter the AMPK pathway. Their combined effect on skeletal muscle energy metabolism, however, is yet to be fully elucidated.

1.4 Adipose tissue dysfunction in obesity

1.4.1 Obesity leads to adipocyte dysfunction

1.4.1.1 Adipose tissue expansion in obesity

White adipose tissue is the largest energy storage organ in the body and stores > 95% of the body's lipids as triglycerides (Large et al. 2004). By storing excess energy, adipose tissue maintains total body lipid and energy homeostasis. In adipocytes, lipoprotein lipase (LPL) catalyses the hydrolysis of circulating chylomicron triglycerides to free fatty acids, which are then re-esterified and subsequently stored as intracellular triglycerides (Large et al. 2004). Adipose tissue triglyceride lipase and hormone-sensitive lipase are the rate-limiting enzymes for the hydrolysis of intracellular triglycerides and DAG respectively (Large et al. 2004; Kershaw et al. 2006). The sequential activation of these lipolytic enzymes results in the release of free fatty acids and glycerol into the circulation. Under normal circumstances, adipose tissue metabolism is tightly coordinated so that energy is stored during the immediate postprandial periods and released during the fasting state in relation to metabolic demand (Yu and Ginsberg 2005). The regulation of energy balance is modulated by both lifestyle (e.g. diet and physical activity) and biological determinants (e.g. genetic and endocrine factors) (Trayhurn 2005). In response to chronic energy excess as in the obese state, increased intracellular lipid accumulation leads to greater adipocyte size (hypertrophy) and the number of adipocytes also increases (hyperplasia) (de Ferranti and Mozaffarian 2008).

1.4.1.2 Adipose tissue expansion leads to adipocyte dysfunction

Adipose hypertrophy and hyperplasia in obesity are associated with an increase in endoplasmic reticulum (ER) stress in adipocytes, which subsequently leads to adipocyte dysfunction. Excessive demands on ER for protein folding, lipid droplet creation and nutrient and cholesterol sensing leads to intracellular accumulation of unfolded protein in adipocytes (de Ferranti and Mozaffarian 2008). ER stress activates inflammatory responses and induces insulin resistance which interferes with normal cellular functions of adipocytes including reduced uptake and storage of fatty acids and dysregulation of cytokine production (Yu and Ginsberg 2005; Gregor and Hotamisligil 2007). In addition, unresolved ER stress and the increased intracellular concentration of free fatty acids lead to oxidative stress in the mitochondria. The subsequent generation of reactive oxygen species (ROS) further impairs adipocyte function and may eventually induce apoptosis (de Ferranti and Mozaffarian 2008).

1.4.2 Inflammation in adipose tissue

1.4.2.1 Obesity is characterised by a chronic inflammatory state

Obesity is associated with a chronic state of low-grade inflammation in both subcutaneous and visceral fat depots (Cancello et al. 2006; Apovian et al. 2008) and an elevated circulating level of inflammatory mediators (Bastard et al. 2006). Epidemiological data suggest that plasma levels of inflammatory markers (e.g. C-reactive protein, tumor necrosis factor (TNF)-α, amyloid A, white blood cells and interleukin (IL)-6) are positively associated with BMI (Panagiotakos et al. 2005). Compared to people with normal fat distribution, the plasma concentrations of inflammatory markers are up to ~ 50% higher in centrally obese individuals (Panagiotakos et al. 2005). *In vitro* visceral adipose tissue explants from obese humans release more biological markers of

inflammation as compared to subcutaneous fat explants (Bruun et al. 2004; Fain et al. 2004).

1.4.2.2 Origin of inflammatory markers in obesity

The inflammatory mediators from adipose tissue are mainly released by infiltrated macrophages and to a lesser extent from mature adipocytes and other cells in the stromal component (e.g. preadipocytes and endothelial cells) (Hauner 2004; Heilbronn and Campbell 2008). The abundance of infiltrated macrophage ranges from 10% in lean to ~ 40% in obese humans and is positively correlated with BMI and adipocyte size (Weisberg et al. 2003). In addition, macrophage infiltration is higher in visceral as compared to subcutaneous fat and the regional variation is consistent in both lean and obese individuals, despite the latter group has 2 – 4 times higher macrophage counts in each fat depot as compared to the lean controls (Harman-Boehm et al. 2007). It should be noted that some inflammatory markers (e.g. TNF-α and plasminogen activator inhibitor (PAI)-1) have lower expression in resting macrophages and their expression increase in response to activation (Ortega Martinez de Victoria et al. 2009). Accordingly, macrophage activation, rather than number, is more relevant to determine the release of inflammatory markers from macrophages.

The underlying cause/s of macrophage infiltration in adipose tissue is/are yet to be fully elucidated. Local adipose hypoxia and adipocyte apoptosis may be a partial explanation. With a limited local oxygen supply, adipocyte hypertrophy and hyperplasia leads to hypoxia which activates cellular stress pathways (de Luca and Olefsky 2008). Subsequently, adipocytes increase the release of chemokines including monocyte chemoattractant protein (MCP)-1 and colony-stimulating factor-1 which are involved in

macrophage recruitment and activation (Cancello and Clement 2006). As a consequence of hypertrophy, necrosis-like adipocyte cell death also attracts macrophages to adipose tissue to scavenge cell debris. The subsequent release of pro-inflammatory cytokines and chemokines from the infiltrated macrophages further contributes to macrophage recruitment (Zeyda and Stulnig 2007) and eventually leads to chronic inflammation of adipose tissue (Harman-Boehm et al. 2007).

1.4.3 Impaired secretory function of adipose tissue in obesity

Protein factors that are specifically expressed and secreted by the adipose tissue (e.g. enzymes, growth factors and cytokines) are collectively known as adipokines (Mora and Pessin 2002). Adipose tissue produces > 100 secretory factors which interact with other tissue types to regulate a range of metabolic and physiologic processes including the modulation of hemostasis, blood pressure, lipid and glucose metabolism, inflammation and atherosclerosis (Hauner 2004; Rabe et al. 2008). An impaired secretion of some of the adipokines, as a consequence of either cellular dysfunction of adipocytes and/or substantial increase in fat mass, is associated with the pathophysiology of obesity-related metabolic abnormalities (Trayhurn 2005). The function of some key adipokines, in particular their relationships with insulin sensitivity and energy metabolism of skeletal muscle, is described below.

1.4.3.1 Leptin

Leptin is produced and released primarily from mature adipocytes and is considered as a metabolic signal for energy sufficiency (Vazquez-Vela et al. 2008). Leptin inhibits food intake and increases energy utilisation by acting as a negative feedback control from adipose tissue to hypothalamus to suppress appetite and increase fatty acid oxidation in

liver and skeletal muscle (Fruhbeck and Salvador 2000). The plasma concentration of leptin is positively correlated with total fat mass (Fruhbeck and Salvador 2000). Compared to subcutaneous fat, visceral fat releases less leptin and the regional difference is consistent in both obese and non-obese individuals (Van Harmelen et al. 1998; Gottschling-Zeller et al. 1999).

Leptin promotes fat oxidation and thus partitions substrates for energy utilisation in skeletal muscle. For example leptin administration (0.5 mg/kg/day for 2 weeks) increased fatty acid oxidation by ~ 2.5-fold in rat oxidative skeletal muscle during contraction (Steinberg et al. 2002). In C2C12 myotubes, a 24 h exposure to leptin increased fatty acid oxidation by up to 26% in a dose-dependent manner (Ramsay 2003). Subcutaneous infusion of leptin (4 mg/kg/day for 5 days) reduced plasma glucose levels in rats, an effect that was associated with an increase in glucose uptake in skeletal muscle (Wang et al. 1999). In high-fat diet-fed rats, a chronic leptin administration (5 mg/kg twice a day for 12 – 15 days) restored whole-body glucose tolerance and insulin-stimulated glucose uptake in skeletal muscle to that of the controls, suggesting the role of leptin in reversing diet-induced insulin resistance (Yaspelkis et al. 2001).

The effect of leptin to increase fat oxidation is at least partly mediated by the selective activation of the AMPKα2 in skeletal muscle. Leptin has been consistently shown to increase the phosphorylation and activation of AMPKα2 *in vivo* (Minokoshi et al. 2002) and *in vitro* (Suzuki et al. 2007). AMPK increases fatty acid oxidation and oxidative capacity of skeletal muscle (Section 1.3.4.3). The activation of the fat oxidative pathway also partitions fatty acids away from lipid accumulation, which is of particular importance to prevent lipid-induced insulin resistance in skeletal muscle. Despite the

effect of leptin on promoting energy utilisation in skeletal muscle, obese individuals are often 'leptin-resistant' as a consequence of reduced bioavailability of leptin (Morris and Rui 2009).

1.4.3.2 Adiponectin

Adiponectin, also known as ApM1, AdipoQ, Acrp30 or GBP28, one of the most abundant adipokines, is produced mainly by mature adipocytes (Lafontan and Viguerie 2006). Full-length (dimer-trimer) adiponectin is the predominant form in the circulation, although the smaller globular fragment generated by proteolytic cleavage is also detected in human serum (Kadowaki and Yamauchi 2005). The circulating level of adiponectin is positively and inversely correlated with insulin sensitivity and adiposity respectively (Lafontan and Viguerie 2006; Hivert et al. 2008). Compared to subcutaneous adipocytes, visceral adipocytes in obese individuals release less adiponectin, whereas no regional variation in adiponectin production has been observed in the lean controls (Drolet et al. 2009). Hypoadiponectinaemia in obese individuals is a consequence of an impaired production and secretion of the adipokine from the enlarged adipocytes, the size of which has been shown to be inversely correlated with adiponectin gene expression (Yang et al. 2004).

Adiponectin increases fatty acid oxidation and has an insulin-sensitising effect on peripheral tissues (Kadowaki and Yamauchi 2005). Incubating mice skeletal muscle with gAcrp30 *ex vivo* increased fatty acid oxidation by up to 19% (Fruebis et al. 2001). In rats, over-expressing adiponectin increased whole-body insulin-stimulated glucose disposal and protected the animals from insulin resistance induced by a high-fat diet (Satoh et al. 2005). The effect of adiponectin on increasing fatty acid oxidation and insulin sensitivity

is partly mediated by AMPK activation (Section 1.3.4.3). An AMPK inhibitor abolished the adiponectin-induced increase in fatty acid oxidation in C2C12 myotubes (Yoon et al. 2006). In skeletal muscle isolated from healthy humans, adiponectin had a synergistic effect on increasing insulin-stimulated glucose uptake and the effect was associated with increased activity of AMPKα1 and α2 (Bruce et al. 2005).

The activation of PPAR-α also mediates the effect of adiponectin on increasing fatty acid oxidation and insulin sensitivity. Adiponectin-induced increase in fatty acid oxidation in C2C12 myotubes was associated with an elevated transcriptional activity of PPAR-α (Yoon et al. 2006). In lipoatrophic mice, adiponectin administration partially alleviated insulin resistance and the effect was associated with increased expression of PPAR-α (Yamauchi et al. 2001). The effect of PPAR-α on up-regulating fatty acid utilisation prevents lipid-induced insulin resistance and subsequently contributes to the insulin-sensitising effect of adiponectin (Lafontan and Viguerie 2006). In addition to the sequential activation of AMPK and PPAR-α, adiponectin also promotes PPAR-α activity via increasing the production of its endogenous ligands in an AMPK-independent manner (Yoon et al. 2006).

1.4.3.3 TNF-α

TNF-α is produced primarily by macrophages and lymphocytes (Antuna-Puente et al. 2008), and modulates a range of processes including host defence, immunity and tissue homeostasis in a manner that is beneficial (Camussi et al. 1991). It is also involved in the pathogenesis of infection, tissue injury and inflammation. The net effect of TNF-α varies depending on the concentration, duration of exposure and the presence of other signalling mediators (Camussi et al. 1991). The circulating level of TNF-α is positively related to

total fat mass (Cartier et al. 2008) and central adiposity (Ziccardi et al. 2002). Although immune cells contribute to the majority of TNF-α released from the adipose tissue, adipocytes also secrete TNF-α and the level of expression is similar in visceral and subcutaneous adipocytes (Good et al. 2006). The correlation between circulating level of TNF-α with central obesity, therefore, is likely a consequence of increased activated macrophages infiltrated in the visceral fat depot (Weisberg et al. 2003).

Epidemiological data suggest that the plasma level of TNF-α is positively correlated with insulin resistance (Hivert et al. 2008). A 4 h TNF-α infusion (1,000 ng/h per m^2) in healthy humans reduced insulin-mediated glucose uptake in skeletal muscle (Plomgaard et al. 2005). In C2C12 myotubes, a 24 h exposure to TNF-α reduced the effect of insulin on increasing glucose uptake by ~ 70% (de Alvaro et al. 2004). Conversely, administrating anti-TNF-α antibody to obese rats increased insulin-stimulated glucose uptake in oxidative skeletal muscle by ~ 70% (Borst et al. 2004). Inhibiting TNF-α signalling via a TNF receptor type 1 blocking peptide in rats fed with a high-fat/high-sucrose diet improved peripheral insulin sensitivity and reduced both weight gain and the weight of epididymal fat pads by ~ 30% (Liang et al. 2008).

The inhibitory effect of TNF-α on the insulin signalling pathway is mediated by multiple pathways. TNF-α activates inhibitor of kappa B kinase (IKK)-β and subsequently leads to serine phosphorylation of IRS-1 which reduces the transduction of insulin-mediated cellular events (de Luca and Olefsky 2008). In primary human myotubes, silencing IKKβ gene expression in TNF-α-treated myotubes completely restored insulin-stimulated glucose uptake to that of the controls (Austin et al. 2008). In addition, TNF-α increases the expression and/or activity of protein-tyrosine phosphatase (PTP)-1B which down-

regulates insulin signalling by dephosphorylating the phosphor-tyrosine residue of the insulin receptor and IRS-1 (Nieto-Vazquez et al. 2008). PTP1B deficiency completely restored insulin sensitivity in TNF-α treated mice and increased insulin-stimulated glucose uptake to ~ 75% of the controls in TNF-α treated myocytes (Nieto-Vazquez et al. 2007).

1.4.3.4 IL-6

In non-acute inflammatory conditions, ~ 15 – 30% of the circulating IL-6 comes from the monocytes and macrophages in the stromal component of adipose tissue (Antuna-Puente et al. 2008). IL-6 mediates the acute phase response to inflammation or tissue injury by inducing the synthesis of acute phase proteins including serum amyloid A and C-reactive protein (Park and Pillinger 2007). The plasma level of IL-6 is positively correlated with total fat mass (Cesari et al. 2005) but with a fat depot-specific effect. The circulating IL-6 level has been shown to be higher in individuals with large visceral depot as compared to those with lesser amount of fat or lean controls (Cartier et al. 2008). *In vitro*, visceral fat releases more IL-6 as compared to subcutaneous fat explant and the regional difference is observed in both lean and obese individuals (Bruun et al. 2004).

IL-6 and insulin sensitivity: acute and chronic effects

Although an elevated circulating level of IL-6 is consistently associated with insulin resistance (Fernandez-Real et al. 2001; Bastard et al. 2002) and has been shown to be an independent predictor of type 2 diabetes (Pradhan et al. 2001), IL-6 appears to have a biphasic effect on insulin sensitivity, which is dependent on the duration of exposure. An acute exposure to IL-6 increases insulin sensitivity. A 4 h IL-6 infusion (5 μg/h) increased insulin-stimulated glucose disposal in healthy humans (Carey et al.

2006). Insulin-stimulated glucose uptake in C2C12 myotubes was further increased by ~ 15% in the presence of an acute IL-6 treatment (25 ng/ml; 3 h) (Nieto-Vazquez et al. 2008). Conversely, chronic IL-6 has been shown to induce insulin resistance. A chronic (1 μl/h for 5 days) IL-6 administration induced a modest degree of whole-body insulin resistance in mice (Klover et al. 2003). A chronic exposure to IL-6 also inhibited insulin-stimulated glucose uptake in a dose-dependent manner in C2C12 myotubes (Nieto-Vazquez et al. 2008). Similarly, net insulin-stimulated glucose uptake in primary human myotubes was completely abolished by a chronic (25 ng/ml; 8 days) exposure to IL-6 (Al-Khalili et al. 2006).

Mechanisms mediating the effect of IL-6 on insulin signalling

The molecular mechanisms by which IL-6 acutely increases insulin sensitivity remain largely unclear. In the presence of insulin, IL-6 increases the association of IRS-1 with the p85 subunit of PI3K and the subsequent insulin-stimulated Akt phosphorylation, an effect concomitant with the activation of AMPK (Carey et al. 2006). In L6 myotubes, a 10 min exposure to IL-6 has been shown to induce the phosphorylation of AMPK in a dose-dependent manner (0 – 100 ng/ml) (Carey et al. 2006). The effect of IL-6 on insulin-stimulated glucose uptake in C2C12 myotubes can be abolished by either a specific AMPK inhibitor or in myotubes infected with an AMPK dominant-negative construct (Nieto-Vazquez et al. 2008).

Exposure to IL-6 for a prolonged period decreases insulin sensitivity, an effect that is mediated by impaired IRS-1 function. IL-6 activates the Janus kinase (JAK)-signal transducers and activators of transcription (STAT) signalling pathway, which induces the activation of NFκB and the mammalian target of rapamycin complex 1

(mTORC1) (Kim et al. 2008; Lam et al. 2008). These events induce the expression of suppressor of cytokine signalling (SOCS)-3, serine phosphorylation and the subsequent degradation of IRS-1 (Flati et al. 2008).

1.4.3.5 Resistin

Activated macrophages are the main source of resistin in adipose tissue (Curat et al. 2006). It has been proposed that resistin is involved in glucose homeostasis, regulation of fat mass and inflammation but the biological role of resistin is still yet to be fully elucidated (Steppan and Lazar 2004). The circulating level of resistin is positively related to the percentage of body fat (Vozarova de Courten et al. 2004). In adipose tissue explants obtained from obese females, visceral fat released 2- to 8-fold more resistin as compared to subcutaneous fat (Fain et al. 2003).

Epidemiological data suggest that the plasma level of resistin is positively related to metabolic risk factors including WHR, plasma triglycerides and a reduction in high-density lipoprotein cholesterol (Norata et al. 2007). No correlation between circulating levels of resistin and insulin sensitivity has been observed in cross-sectional analyses (Azuma et al. 2003; Norata et al. 2007). In contrast, a longitudinal study of a 1.5 yr weight reduction program showed that the decrease in plasma resistin level was associated with an improvement in insulin sensitivity in obese non-diabetic subjects (Azuma et al. 2003).

Over-expressing resistin induced whole-body insulin resistance in rats and the effect was associated with reduced insulin-stimulated IRS-1 and Akt activation in skeletal muscle (Satoh et al. 2004). Similarly, resistin inhibited the effect of insulin on increasing

glycogen synthesis in skeletal muscle isolated from spontaneously hypertensive rats (Pravenec et al. 2003). In L6 myotubes, resistin reduced insulin-stimulated glucose uptake in L6 myotubes in a dose-dependent manner (Moon et al. 2003). In contrast, despite being a biomarker and potentially a mediator of inflammatory response, the direct role of resistin, if any, in the pathophysiology of insulin resistance in human remains unclear (Lazar 2007).

1.4.3.6 PAI-1

PAI-1 is a fibrinolytic inhibitor which maintains blood vessel patency by regulating cell adhesion and migration (Alessi and Juhan-Vague 2006). While endothelial and vascular smooth muscle cells are the main sources of PAI-1, adipocytes and cells from the stromal component of the adipose tissue have also been shown to secrete the cytokine (Correia and Haynes 2006). The circulating level of PAI-1 is positively correlated with total fat mass (Godsland et al. 2005). In healthy pre-menopausal women, plasma PAI-1 level was positively related to visceral but not subcutaneous fat area (Janand-Delenne et al. 1998). In adipose tissue explants from obese humans, PAI-1 production is mainly due to stromal cells (Bastelica et al. 2002) and visceral fat released twice as much PAI-1 as from subcutaneous fat (Fain et al. 2004).

The circulating level of PAI-1 is positively correlated with insulin resistance in asymptomatic individuals (Godsland et al. 2005) and type 2 diabetic patients (Aso et al. 2005). Epidemiological data suggest that elevated circulating level of PAI-1 is a strong risk factor for type 2 diabetes independent of body fat and insulin resistance (Festa et al. 2002). It has been proposed that PAI-1 may merely be a consequence of obesity and insulin resistance as the associated metabolic disorders (e.g. hyperinsulinaemia,

dylipidaemia and impaired glucose tolerance) are known to stimulate PAI-1 release and therefore contribute to the relationship between PAI-1 and insulin resistance (Bastard et al. 2000). The protective effect of PAI-1 deficiency against high-fat diet-induced obesity and insulin resistance in mice, however, suggests a possible causal role of PAI-1 in insulin resistance (Ma et al. 2004). There is some evidence that PAI-1 regulates adipose tissue function which may subsequently modify whole-body insulin sensitivity *in vivo* (Ma et al. 2004). The direct effect, if any, of PAI-1 on insulin signalling and energy metabolism in skeletal muscle is yet to be determined.

1.4.3.7 IL-8

The chemokine IL-8 exhibits both neutrophil and lymphocyte chemotactic activity and is involved in the pathogenesis of atherosclerosis and cardiovascular disease (Driscoll et al. 1997; Bruun et al. 2004). IL-8 secreted from adipose tissue is mainly released from monocytes and macrophages and to a lesser extent from adipocytes (Bruun et al. 2004). The circulating level of IL-8 is positively related to total fat mass (Straczkowski et al. 2002). In obese individuals, plasma IL-8 level is also positively correlated with WHR and IL-8 levels in centrally obese subjects were ~ 30% higher as compared to the peripherally obese group (Straczkowski et al. 2002). This is consistent with the higher IL-8 release from visceral as compared to subcutaneous fat explants *in vitro* (Bruun et al. 2004).

The relationship between IL-8 level and insulin sensitivity is unclear. Epidemiological data suggest that serum level of IL-8 is closely associated with risk for type 2 diabetes (Herder et al. 2006). In obese individuals, the plasma level of IL-8 was marginally associated with insulin resistance (P = 0.05) (Bruun et al. 2003). Diet-induced weight

loss improved insulin sensitivity, reduced TNF-α and IL-6 but increased IL-8 in the circulation (Bruun et al. 2003). Recently IL-8 has been shown to inhibit insulin-stimulated Akt phosphorylation in human adipocytes via the activation of the mitogen-activated protein kinase (MAPK) pathway (Kobashi et al. 2009). The direct effect of IL-8, if any, on insulin sensitivity in skeletal muscle is yet to be determined.

1.4.3.8 The combined effect of adipokines determines adipose tissue function

Given the fact that adipokines modify muscle energy metabolism via both common and distinct mechanisms and some have opposite effects on particular metabolic pathways, the overall function of adipose tissue under physiological condition is determined by the net effect of all the secretory factors from both adipocytes and stromal cells. Accordingly, defining the effect of an individual adipokine in isolation is of limited physiological relevance. The development of a model to understand the *in vivo* interactions amongst the adipokines would be of significant importance to determine adipose tissue function and its interaction with other tissue types (Section 1.6.3).

1.5 The effect of long-chain fatty acids on energy metabolism in skeletal muscle

1.5.1 Structural characteristics of fatty acids determine their metabolic roles

In addition to being an energy substrate, free fatty acids are important signalling molecules and are actively involved in the regulation of energy metabolism. Various types of fatty acids are metabolised differently. For example saturated fatty acids (SFAs) tend to be converted into lipid metabolites whereas the unsaturated ones are more likely to undergo oxidation (Gaster et al. 2005; Lee et al. 2006). The metabolic characteristics of fatty acids depend on their chain lengths and the number, position and the geometry (*cis* or *trans*) of the double bonds (Katan et al. 1994), which subsequently modify their

physical properties and specificity for enzymes involved in particular metabolic pathways (Gaster et al. 2005). In the following section, the specific effects of long-chain saturated (contain no double bond), monounsaturated (contain one double bond) and polyunsaturated (contain ≥ 2 double bonds) fatty acids on energy metabolism, in particular insulin sensitivity, of skeletal muscle is reviewed.

1.5.2 Long-chain saturated fatty acids

1.5.2.1 SFAs induce insulin resistance

Saturated fat accounts for ~ 15% of energy in the average American diet (German and Dillard 2004). Palmitic acid (PA; 16:0) and stearic acid (18:0) are the two main dietary saturated fatty acids (Katan et al. 1994). Saturated fat intake is associated with an impairment of insulin action and is a long-term predictor of insulin resistance and metabolic syndrome (Riccardi et al. 2004; Riserus et al. 2007). A 90-day intervention with a high-saturated fat diet (17% of total energy) reduced insulin sensitivity in healthy humans (Vessby et al. 2001). Similarly, a 12 h exposure to either PA or stearic acid abolished insulin-stimulated glucose uptake in primary human myotubes (Montell et al. 2001). These data provide direct evidence for the effect of SFAs on inducing insulin resistance in skeletal muscle.

1.5.2.2 Molecular mechanisms of SFA-induced insulin resistance

The inhibitory effect of SFAs on insulin sensitivity is mediated by the accumulation of lipid metabolites, for example ceramide and DAG in skeletal muscle (Section 1.3.3.2). In C2C12 myotubes, PA inhibited insulin-stimulated Akt phosphorylation, an effect prevented by abolishing the *de novo* synthesis of ceramide using a specific SPT inhibitor (Chavez et al. 2003). Incubating C2C12 myotubes with either PA or stearic acid induced

a 3-fold increase in intramuscular ceramide content whereas monounsaturated derivatives of the fatty acids were without effect (Chavez et al. 2003). The unique effect of saturated fatty acids on inducing intramuscular ceramide accumulation is a consequence of the substrate specificity of SPT, which is highly selective for long-chain saturated fatty acyl-CoAs (Hanada 2003; Straczkowski and Kowalska 2008). Palmitoyl-CoA is one of the most abundant acyl-CoAs in mammalian cells and is also the best substrate of SPT *in vitro* (Hanada 2003).

There is evidence that DAG mediates the inhibitory effect of SFAs on insulin sensitivity in skeletal muscle. Rats fed with a high-saturated fat diet were insulin-resistant and had ~ 2.5-fold higher intramuscular DAG content as compared to standard diet controls (Lee et al. 2006). In C2C12 myotubes, the inhibitory effect of PA and stearic acid on insulin-stimulated Akt activation was associated with an increase in DAG accumulation by up to 6-fold (Chavez et al. 2003).

The pathways mediating the inhibitory effect of SFAs on insulin-stimulated glucose uptake in skeletal muscle are summarised in Figure 1.7. The relative role of ceramide and DAG on mediating SFA-induced insulin resistance is unclear. It has been proposed that the inhibitory effect of DAG on insulin sensitivity may be unimportant. Abolishing *de novo* synthesis of ceramide has been consistently shown to be sufficient to restore insulin sensitivity in PA-treated skeletal muscle cells despite no change or even a further increase in DAG accumulation (Chavez et al. 2003; Powell et al. 2004; Pickersgill et al. 2007).

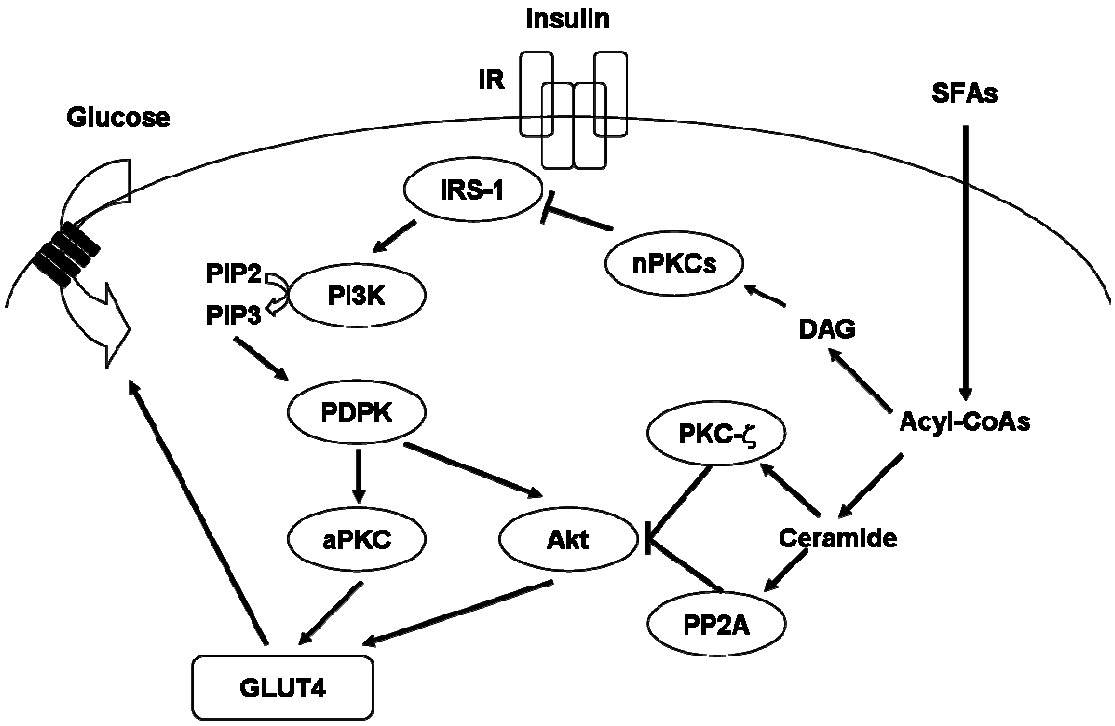

Figure 1.7. Pathways mediating the inhibitory effect of saturated fatty acids (SFAs) on insulin-stimulated glucose uptake in skeletal muscle. SFAs increase intramuscular content of ceramide and diacylglycerol (DAG). Ceramide increases protein kinase C (PKC)-ζ activity which impairs insulin-stimulated Akt activation. In addition, ceramide desensitises the effect of insulin on Akt activation by accelerating Akt dephosphorylation via protein phosphatase (PP)-2A. DAG activates DAG-sensitive novel PKCs (nPKCs) which then leads to serine phosphorylation of insulin receptor substrate (IRS)-1.

1.5.2.3 SFAs promotes lipid storage

SFAs promote triglyceride accumulation in skeletal muscle. Rats fed with a high-fat diet consisting of primarily SFAs had ~ 50% higher intramuscular triglyceride as compared to rats fed with a standard chow (Lee et al. 2006). In L6 myotubes, triglyceride accumulation increased by ~ 20% in response to PA (Lee et al. 2006). The effect of SFAs on increasing triglyceride synthesis in skeletal muscle is at least in part due to increased expression and activity of the Δ9 desaturase stearoy-coenzyme A desaturase (SCD). SCD1, and to a lesser extent SCD2 are the predominant isoforms of the SCD genes expressed in skeletal muscle (Dobrzyn and Dobrzyn 2006). The long-chain saturated fatty acyl-CoAs are preferred substrates for SCD. The products of SCD, mainly palmitoleoyl- and oleoyl-CoA, are the major components of tissue lipids including triglycerides, cholesteryl esters and phospholipids (Dobrzyn and Dobrzyn 2006). In response to a high saturated-fat diet, the activity, mRNA and protein content of SCD increased and triglycerides accumulated in rat skeletal muscle (Lee et al. 2006). Similarly, PA increased SCD1 mRNA content in L6 myotubes (Voss et al. 2005). The direct effect of SCD on triglyceride accumulation was demonstrated by over-expressing SCD1 in L6 myotubes, in which intramuscular triglyceride content was increased by 40% (Pinnamaneni et al. 2006).

It has been proposed that the effect of SFAs on promoting triglyceride accumulation is a protective mechanism against the accumulation of lipid metabolites and the subsequent lipid-induced insulin resistance (Pinnamaneni et al. 2006). The effect of SCD on fatty acid metabolism and insulin sensitivity in skeletal muscle, however, is controversial. SCD1 mRNA content in PA-treated primary human myotubes *in vitro* has been shown to be positively related with insulin sensitivity of the muscle donors *in vivo* (Peter et al.

2009). In L6 myotubes, over-expressing SCD1 partially reversed the inhibitory effect of PA on insulin-stimulated Akt activation and glucose uptake, an effect that was associated with an increase in intramuscular triglyceride content and a reduction in ceramide and DAG accumulation (Pinnamaneni et al. 2006). In contrast, SCD1-deficient mice have also been shown to have reduced intramuscular ceramide content which was associated with an increase in fatty acid oxidation in skeletal muscle (Dobrzyn et al. 2005). These data clearly suggest that as an important regulator of triglyceride synthesis, SCD modifies the partitioning of SFAs towards oxidation and lipid metabolite accumulation. The direct relationship between factors modifying SCD expression and/or activity, for example fatty acids of various degrees of saturation and potentially adipokines, and energy metabolism and insulin sensitivity in skeletal muscle is yet to be determined.

1.5.3 Long-chain monounsaturated fatty acids (MUFAs)

1.5.3.1 MUFAs and insulin sensitivity

Monounsaturated fat accounts for 30 – 40% of dietary fat in the western diet and oleic acid (18:1n-9) is the main dietary MUFA (Katan et al. 1994). Population studies suggest that insulin resistance is inversely related to dietary intake of oleic acid from cooking oil (Soriguer et al. 2004). A Mediterranean diet, with olive oil (~ 70% fatty acids as oleic acid) as the primary fat source (Kien et al. 2005), is inversely related to insulin resistance in healthy humans (Panagiotakos et al. 2007), and modestly associated with higher insulin sensitivity, better lipid profile, and lower blood pressures in overweight and obese people (Tzima et al. 2007). In contrast to these epidemiological data, a 3-month intervention with a diet high in MUFA (23% of energy) did not affect insulin sensitivity in healthy humans (Vessby et al. 2001). The results of the population studies may be important because a high-MUFA (23% energy) weight maintenance diet has been shown

to improve insulin sensitivity in obese insulin-resistant subjects (Paniagua et al. 2007). In skeletal muscle cells, oleic acid had no effect on insulin sensitivity but attenuated the inhibitory effect of PA on insulin-stimulated Akt phosphorylation (Coll et al. 2008) and glucose uptake (Montell et al. 2001). These data suggest that MUFAs only improve insulin sensitivity in the context of pre-existing insulin resistance.

1.5.3.2 MUFAs attenuate insulin resistance by promoting fatty acid oxidation

The effect of MUFAs on attenuating insulin resistance is mediated by partitioning fatty acids away from the synthesis of lipid metabolites in skeletal muscle. In C2C12 myotubes, the effect of oleic acid on reducing PA-induced insulin resistance was associated with a decrease in intramuscular DAG accumulation, which has been proposed to be a consequence of partitioning PA towards fatty acid oxidation (Coll et al. 2008). There is some evidence that MUFAs promote fat oxidation. In overweight but otherwise healthy men, the postprandial fat oxidation rate following a high-MUFA meal was higher as compared to an isocaloric high-SFA meal (Piers et al. 2002). Oleic acid induced CPT-I mRNA in C2C12 myotubes and the effect remained in the presence of PA which was without effect by itself (Coll et al. 2008). A high-MUFA diet, however, did not affect plasma triglyceride levels in overweight/obese non-insulin-dependent diabetic patients (Luscombe et al. 1999).

Under conditions in which MUFAs are contributing to weight gain, the beneficial effect on insulin sensitivity is lost. In rats, a 12-week intervention with a high-fat diet, primarily of MUFAs, has been shown to induce obesity and insulin resistance to a similar extent as occurred in control rats fed with a high-SFA diet (Buettner et al. 2006). Accordingly,

MUFAs have beneficial effects on insulin sensitivity and energy metabolism in the context of energy homoeostasis, and when replacing SFAs such as PA.

1.5.4 Long-chain polyunsaturated fatty acids

PUFAs are categorised as n-3 and n-6 based on the location of the last double bond relative to the terminal methyl end of the fatty acid (Schmitz and Ecker 2008). In the western diet, the common source of n-3 PUFAs are α-linolenic acid (18:3n-3) of plant origin and eicosapentaenoic acid (EPA) and docosahexaenoic acid (DHA) of marine origin (Katan et al. 1994). Linoleic acid (LA; 18:2n-6) is the main dietary n-6 PUFAs (Katan et al. 1994). According to a review by Schmitz and Ecker (2008), both n-3 and n-6 PUFAs are precursors of signalling molecules that regulate cellular functions including inflammation and lipid metabolism. Once transported into the cytoplasm, both n-3 and n-6 PUFAs are metabolised by the same group of desaturases and elongases. Therefore the metabolism and physiological functions of n-3 and n-6 PUFAs are partly dependent on the relative abundance of these two types of fatty acids (Schmitz and Ecker 2008).

Consumption of n-3 PUFAs, in particular those of marine origin, have been associated with improved insulin sensitivity. In an elderly population, fish intake was inversely correlated with the risk of developing impaired glucose tolerance and diabetes, a relationship independent of age, sex and BMI (Feskens et al. 1991). Supplementing an energy-restricted diet (70% of normal energy intake) with fish oil capsules (6 x 500 mg capsules/day) for 8 weeks improved insulin sensitivity in overweight and obese young adults, an effect not accounted for by weight loss or reduction in plasma triglyceride (Ramel et al. 2008). Similarly, the effect of substituting n-3 PUFAs for SFAs on

preventing diet-induced insulin resistance has been consistently demonstrated in animal models (Delarue et al. 2004).

The effect of n-3 PUFAs on improving insulin sensitivity is at least partly due to the modified fatty acid composition in the muscle membrane phospholipids (Storlien et al. 1991). The PUFA acyl chains are extremely flexible and increase membrane fluidity, which subsequently modify the activity of membrane bound proteins (Schmitz and Ecker 2008). n-3 PUFAs in the membrane phospholipids increase insulin binding to its receptor (Liu et al. 1994) and activation and/or catalytic capacity of insulin receptor kinase (Nadiv et al. 1994), which subsequently improves insulin action on skeletal muscle.

In rats fed with a high-fat diet, n-3 PUFAs reduced plasma triglycerides and hepatic lipid content (Neschen et al. 2002; Hong et al. 2003). Similarly, replacing 10% of the saturated fat with n-3 PUFAs in a high-fat diet reduced plasma triglycerides and improved insulin action in rats (Ukropec et al. 2003). n-3 PUFAs reduce triglyceride accumulation by a combined effect of promoting fatty acid oxidation and reducing lipogenesis (Section 6.1). Briefly, n-3 PUFAs activate PPAR-α (Forman et al. 1997) which increases fatty acid oxidation (Section 1.3.4.3). n-3 PUFAs also inhibit the gene expression and activation of nuclear sterol regulatory element binding protein (SREBP)-1 and subsequently reduce the transcription of a range of lipogenic genes (Schmitz and Ecker 2008).

n-6 PUFAs share some common effects with n-3 PUFAs such as increasing membrane fluidity (Schmitz and Ecker 2008) and fatty acid oxidation (Javadi et al. 2007) (Section 6.1). In contrast to n-3 PUFAs, the effect of n-6 PUFAs on insulin sensitivity is less well-defined. Compared to standard chow controls, rats fed with a high-fat diet consisting

primarily of LA induced a small and yet significant increase in insulin sensitivity (Lee et al. 2006). Substituting LA-enriched oils and margarines for saturated fats, however, had no effect on fasting blood glucose and glycosylated haemoglobin in type 2 diabetic patients (Heine et al. 1989). The relative effects of n-3 and n-6 PUFAs on insulin sensitivity and the mechanisms by which they occur have not been previously studied.

Despite evidence for the beneficial effects of PUFAs on fatty acid utilisation and insulin sensitivity *in vivo* in animals and humans, the data relating to the mechanisms were obtained in liver; the effects of n-3 and n-6 PUFAs in skeletal muscle remain unclear. In addition, under physiological conditions skeletal muscle metabolism is under the influence of multiple factors including different types of fatty acids and numerous adipokines from the adipose tissue. The complexity of factors regulating energy metabolism and insulin sensitivity of skeletal muscle makes it difficult to understand the interactions between them in *in vivo* studies. *In vitro* models are useful to isolate factors of interest but often are of limited physiological relevance. This implicates the need to establish novel *in vitro* systems which preserve *in vivo* interactions and at the same time enable the identification of factors of potential significance in metabolism.

1.6 *In vitro* systems to study adipose tissue-skeletal muscle interactions

1.6.1 An overview of co-culture systems to study tissue interactions *in vitro*

Communication between various cell types plays an important role in regulating tissue functions. In co-culture systems, mixing known composition of different cell populations mimics cell-to-cell interactions or paracrine/autocrine relationships *in vitro* (Hausman and Poulos 2005). Co-cultures have been commonly used to study angiogenesis (Bader et

al. 1996), dynamics of blood-brain barrier (Nehls and Drenckhahn 1995) and immune cell function (Ternaux and Portalier 1996).

Various co-culture systems have been developed to study tissue interactions of different nature. Culturing a mixed cell population on a single plane allows physical contact between the cells which may affect cell function (Dodson et al. 1997). Where the aim of the co-culture is to study the effect of soluble secretory factors on other cell types, the different cell types may be cultured on separate surfaces and establish the co-culture in a shared medium (Dietze et al. 2002). Incubating cell culture with conditioned medium from another cell type is an indirect approach of co-culture, which is particularly useful to eliminate confounding variables when both cell types are affected by the experimental conditions (Dietze et al. 2004).

1.6.2 Limitations of the existing adipocyte-myotube co-culture models

Given the effect of adipokines (Section 1.4.3) and fatty acids (Section 1.5) on energy metabolism in skeletal muscle, *in vitro* co-culture systems have been used in an attempt to elucidate the effect of adipose tissue on muscle insulin sensitivity although with somewhat contradictory findings. Dietze et al (2002) and Sell et al (2008) examined the effect of mammary fat on insulin-stimulated Akt phosphorylation by co-culturing primary human myotubes with preadipocytes isolated from human mammary adipose tissue. Dietze et al (2002) showed that secretory factors from adipocytes abolished insulin-stimulated Akt activation, whereas Sell et al (2008) demonstrated the effect of insulin on increasing Akt phosphorylation in the presence of adipocyte-conditioned medium. While an inverse relationship between visceral fat mass and insulin-stimulated glucose disposal in skeletal muscle has been consistently demonstrated *in vivo* (Colberg

et al. 1995; Virtanen et al. 2005), Vu et al (2007) showed that the co-culture of primary rat visceral adipocytes with L6 myotubes increased glucose uptake, an effect associated with increased activation of IRS-1, Akt and AMPK. The limited reproducibility of the effect of adipokines on muscle insulin sensitivity and the discrepancy between findings from *in vitro* and *in vivo* studies raise questions about the nature of adipose tissue-skeletal muscle interactions of the *in vitro* co-culture systems used to study them.

The major limitation of the above co-culture systems is not able to mimic the *in vivo* crosstalk between adipose tissue and skeletal muscle. Over 90% of secretory factors released from the adipose tissue originate from non-fat cells (Fain et al. 2004). Accordingly, any influence of adipose tissue on metabolism under physiological conditions is in fact a combined effect from all adipose tissue-derived factors, and preserving the *in vivo* crosstalk between various cell types in the tissue is crucial when using *in vitro* models to study adipose tissue function (Thalmann et al. 2008). This is particularly important in the study of adipose tissue-skeletal muscle interactions as the stromal cells, in particular the activated macrophages, are an important source of adipokines, which are known to modify energy metabolism and insulin sensitivity in skeletal muscle (Section 1.4.3). Using isolated adipocytes to establish co-cultures with skeletal muscle cells, therefore, is of limited physiological relevance.

1.6.3 A novel system to study adipose tissue-skeletal muscle interactions *in vitro*

Culturing skeletal muscle cells with adipose tissue-conditioned media is a novel indirect co-culture system to study adipose tissue-skeletal muscle interactions *in vitro*. The components and the advantages of the model will be described below.

1.6.3.1 Skeletal muscle cells

An overview of skeletal muscle cell culture

Cultured myotubes express protein and functional characteristics of skeletal muscle and are widely used to study the effects of various factors including nutrients (Perriott et al. 2001; Chavez et al. 2003), adipokines (Al-Khalili et al. 2006) and pharmacological agents (Fediuc et al. 2008) on muscle metabolism. Myoblasts are maintained in the proliferative phase and, when reaching confluence, induced to differentiate into myotubes by depriving the cultures of growth factor. During differentiation, the mononucleated myoblasts stop dividing, fuse into multinucleated myotubes and activate the expression of muscle-specific genes (Stern-Straeter et al. 2008). The extent of differentiation into myotubes is confirmed microscopically by observing multinucleated myotube formation or biochemically by determining the activity of creatine phosphokinase and/or the presence of sarcomeric actin (Lawson and Purslow 2000).

Human primary myotubes

Primary skeletal muscle cell culture is established from isolated satellite cells, positioned between the basement membrane and the sarcoplasmic reticulum of muscle fibres, which retain the ability to proliferate and regenerate muscle in appropriate culturing conditions (Blau and Wester 1981). Human primary myotubes are particularly useful in determining the specific biochemical and genetic basis of insulin resistance in skeletal muscle, which is often complicated by secondary metabolic changes including chronic hyperglycaemia, lipid abnormalities and pre-existing hyperinsulinaemia (Jackson et al. 2000). In addition, primary cell cultures established from type 2 diabetic patients, obese

and healthy individuals have been shown to reflect the metabolic characteristics of the muscle donors and therefore provides an opportunity to determine the role of intrinsic defects of skeletal muscle in insulin resistance (Gaster et al. 2002; Chen et al. 2005; Ukropcova et al. 2005).

Primary cell cultures have several major limitations. First, primary myotubes lose proliferative capacity and phenotype as the culture passages. Satellite cells proliferate at a high initial rate, followed by a gradual loss of proliferative potential and eventually the cells will stop dividing (Renault et al. 2000). In primary human cell lines, insulin sensitivity was maintained through 9 – 10 population doublings and the effect of insulin on increasing glycogen production was progressively lost in further passages (Thompson et al. 1996). Second, contamination with non-muscle cells, in particular fibroblasts, affects the specificity of the cell culture response (Thompson et al. 1996). Fibroblasts are selectively removed by pre-plating myoblasts on plastic cultureware, during which the fibroblasts would attach to the surface while most of the myoblasts would remain floating in the medium (Yaffe 1968). Muscle-specific culture may also be confirmed by the expression and/or activity of muscle-specific proteins (Thompson et al. 1996). Finally, the fibre composition of the muscle of origin is not preserved in human satellite cell cultures (Rosenblatt et al. 1996). Human myotubes co-express both fast and slow myosin heavy chains irrespective of the fibre type of the muscle from which they originate (Bonavaud et al. 2001). Accordingly, the potential use of human primary cell culture to determine fibre type-specific characteristics of muscle is limited.

L6 myotubes

L6 is a myogenic cell line of rat origin first developed by Yaffe (1968) and is commonly used as an alternative to primary muscle cell cultures. The advantages of myogenic cell lines over primary cell cultures include easy storage, good growth and they are able to maintain in a continuous state of replication without the loss of differentiation potential and stereotypical results (Bonavaud et al. 1997).

L6 cells have been commonly used to investigate insulin-stimulated glucose metabolism in a cellular model of skeletal muscle due to their high sensitivity and responsiveness to insulin stimulation (Huang et al. 2002; Ceddia et al. 2005). Once differentiated, the myotubes develop a fully functional insulin-signalling cascade including the protein expression of GLUT4, insulin receptor and IRS-1 (Lamphere and Lienhard 1992), high affinity and specificity binding of insulin to its receptors (Beguinot et al. 1986) and the translocation of GLUT4 proteins to the plasma membrane in response to insulin (Koivisto et al. 1991). Cultures from myogenic cell lines are often used in initial studies, with the results later verified using primary muscle cell cultures (Bonavaud et al. 1997).

1.6.3.2 Adipose tissue-conditioned media

Adipose tissue-conditioned media is possibly the most physiologically relevant way to demonstrate the secretory function of adipose tissue in an *in vitro* model. Adipose tissue explants have previously been used to study depot-specific effects of lipolysis (Fried et al. 1993) and adipokine secretion (Fain et al. 2004) *in vitro*. Generating conditioned media from adipose tissue explants not only captures all secretory factors from the whole

tissue, but the proportion of different cell types in the tissue explant is also preserved so that the adipokine profile in the conditioned media resembles that is released from the tissue under physiological conditions. Accordingly, culturing skeletal muscle cells with adipose tissue-conditioned media preserves the net effect of adipose tissue on muscle metabolism.

Secretory factors from adipose tissue modify skeletal muscle metabolism via both common and distinct mechanisms and the use of conditioned media helps identify the cytokines of interest. For example the contribution of a particular cytokine towards the overall function of adipose tissue may be determined by neutralising the biological activity of the cytokine using a specific antibody. Conversely, re-constituting the conditioned media using individual or combinations of cytokines is an alternative way to determine the interactions of cytokines in adipose tissue function.

1.6.3.3 Potential use of the adipose tissue-conditioned media-myotube system

Under physiological conditions, skeletal muscle is under the influence of adipokines as well as other hormones and nutrients. The relatively simple assembly of the proposed adipose tissue-conditioned media-myotube culture facilitates the inclusion of other factors in the system to demonstrate the effect of their interactions with adipokines on muscle metabolism. For example dysregulated adipokine secretion and elevated circulating levels of free fatty acids have both been associated with insulin resistance in obesity and the combined effect of the two on insulin sensitivity in skeletal muscle may be mimicked in the proposed system. Accordingly, the system is useful to study other complex interactions regulating skeletal muscle metabolism *in vitro*.

1.7 Aims

The overall aim of this study was to determine the effect of subcutaneous and visceral fat, long-chain saturated, n-3 and n-6 PUFAs, and their interactions, on insulin sensitivity and pathways regulating energy metabolism in skeletal muscle and the possible mechanisms involved.

The specific aims of the studies were as follows:

1. To develop an *in vitro* system to study the effect of secretory factors from adipose tissue on basal and insulin-stimulated glucose uptake in skeletal muscle cells using adipose tissue-conditioned media
2. To determine the effect of subcutaneous and visceral fat on basal and insulin-stimulated glucose uptake in skeletal muscle *in vitro* and the mechanisms involved
3. To determine the effect of long-chain saturated, n-3 and n-6 PUFAs and their interactions with secretory factors from subcutaneous and visceral fat on basal and insulin-stimulated glucose uptake in skeletal muscle in vitro and the mechanisms involved
4. To determine the effect of long-chain saturated, n-3 and n-6 PUFAs and their interactions with secretory factors from subcutaneous and visceral fat on pathways regulating energy metabolism in skeletal muscle in vitro
5. To determine the effect of long-chain saturated and n-3 PUFAs on gene expression profile in skeletal muscle in vitro

Chapter 2: Methodology

2.1 Collection of human skeletal muscle and adipose tissue biopsies

Rectus abdominus muscle, abdominal subcutaneous (SC) and visceral omental (IAB) adipose tissue explants were obtained from lean and obese patients who were undergoing hernia surgery or gastric bypass surgery for the treatment of morbid obesity respectively. The collection of tissue samples was approved by the human research ethics committees of the University of Adelaide, Royal Adelaide Hospital, Calvary North Adelaide Hospital and Burnside Hospital and was performed by qualified surgeons. Informed consent was given by all patients prior to collection of tissue.

2.2 Skeletal muscle cell culture

2.2.1 L6 cells

The L6 cell line (at passage 7 in freezing medium containing 10% dimethyl sulfoxide (DMSO; v/v)) was a gift from the Metabolic Research Unit of Deakin University and was stored in liquid nitrogen until use. L6 cell cultures were developed according to methods described by Mitsumoto and Klip (1992) and Lawson and Purslow (2000). All solutions were warmed to 37°C prior to use unless specified and aseptic techniques in a biological safety cabinet were used for all procedures.

An ampule of L6 cells (1 ml) was rapidly thawed in a 37°C water bath and the cells were then added to a 75 cm^2 CELLSTAR® filter cap cell culture flask (Greiner Bio-One #658175 distributed by Interpath Services Pty Ltd, Heidelberg West, Victoria, Australia) containing 9 ml of growth medium (Minimum Essential Medium Alpha Modification (α-MEM; Sigma-Aldrich #51452C, Lenexa, Kansas, USA) supplemented with 10% Fetal

Bovine Serum (FBS; SAFC Biosciences #12203C distributed by Sigma-Aldrich, Castle Hill, New South Wales, Australia; v/v), 50 U/ml penicillin and 50 μg/ml streptomycin (Sigma-Aldrich #P4458, St Louis, Missouri, USA)). The flask was incubated at 37°C for 2 h to allow cells to adhere to the flask, after which the medium was discarded and replaced by fresh growth medium. The cells were kept in an atmosphere of 5% carbon dioxide (CO_2) at 37°C and the growth medium was refreshed every 48 h until 70% confluence. Thereafter, the cells were washed twice with sterile phosphate buffered saline (PBS) prepared by dilution of 10x Dulbecco's Phosphate Buffered Saline (Sigma-Aldrich #D1408) with deionised water and dissociated by adding 3 ml of 0.05% trypsin-ethylenediaminetetraacetic acid disodium salt dihydrate (EDTA) (Sigma-Aldrich #59417C; w/v). After incubation at 37°C for 3 min, 7 ml of growth medium was then added to inactivate the trypsin. The dissociated cells were split using a ratio of 1:10 – 1:40 with growth medium for experiments at passages 9 – 24.

Depending on the experiment, cells were seeded on 6-well plates (Greiner Bio-One #657160; 2 ml/well), 12-well plates (Greiner Bio-One #665180; 1 ml/well) or Petri dishes (Greiner Bio-One #664160; 5 ml/dish) and maintained in growth medium. At 70% confluence, the cells were differentiated into myotubes by replacing the culture medium with α-MEM containing 2% horse serum (HS; SAFC Biosciences #12449C distributed by Sigma-Aldrich; v/v), 50 U/ml penicillin and 50 μg/ml streptomycin. The cells were kept in the differentiation medium for 3 days and the differentiation of cells into myotubes was confirmed by visualisation of myotube formation under light microscopy. The myotubes were rinsed twice with serum-free medium (α-MEM supplemented with 0.1% Bovine Serum Albumin (BSA; Sigma-Aldrich #A1470; w/v)) prior to treatments.

2.2.2 Primary human skeletal muscle cells

Human primary skeletal muscle cell culture was developed according to methods described by Blau and Webster (1981) and modified by Gaster et al (2001). All solutions were warmed to 37°C prior to use unless specified and aseptic techniques in a biological safety cabinet were used for all procedures.

A 25 cm^2 CELLSTAR® filter cap cell culture flask (Greiner Bio-One #690175) was coated with 1.3% extracellular matrix (ECM; Sigma-Aldrich #E1270; v/v) gel. The ECM gel was used as a cell culture substratum. The major constituents, laminin, collagen type IV, heparan sulphate proteoglycan and entactin are cell adhesion factors which facilitate the attachment of muscle cells to glass or plastic. The 5 ml ECM gel from the manufacturer was thawed to 4°C overnight and diluted in 70 ml of growth medium (α-MEM supplemented with 10% FBS (v/v), 25 U/ml penicillin, 25 µg/ml streptomycin and 3 µg/ml amphotericin B (Sigma-Aldrich #A9528)), which was then divided into 1 ml aliquots and stored at -20°C until use. Ice-cold growth medium (4 ml) was added to an aliquot of ECM gel and the diluted gel was kept at 4°C prior to dispensing to the flask. The excess gel was removed and the coating was allowed to sit at room temperature for 2 h before cells were plated.

After removing visible connective tissues and blood vessels, the muscle tissue (approximately 50 – 100 mg w.w.) was immediately placed in ice-cold α-MEM and transported to the laboratory on ice, rinsed 3 times in ice-cold α-MEM and then transferred to a Petri dish, in which 3 ml of 0.05% trypsin-EDTA (w/v) was added and the tissue was minced to a fine paste with a scalpel. Muscle cells were dissociated by 3 successive 20 min incubations with 15 ml of 0.05% trypsin-EDTA (w/v) in a sterile 50

ml Erlenmeyer flask (Schott Australia, Frenchs Forest, New South Wales, Australia) with constant agitation at room temperature. After each 20 min incubation, the supernatant was pooled in a 50 ml conical tube (Greiner Bio-One #227270) containing 5 ml of ice-cold HS to inactivate enzymatic digestion and was kept on ice. The combined supernatant was strained using a 100 μm cell strainer (BD Biosciences #352360, Bedford, Massachusetts, USA) to remove any remaining clumps of tissue and the cell suspension was centrifuged at 1,600 rpm for 7 min at room temperature. The cell pellet was resuspended in 5 ml of growth medium. The cells were pre-plated in an uncoated 25 cm^2 CELLSTAR® filter cap cell culture flask and incubated at 37°C for 20 min to reduce fibroblast content in the cell culture. The cells were then seeded in an ECM gel-coated 25 cm^2 CELLSTAR® filter cap cell culture flask. The cells (passage 1) were maintained in an atmosphere of 5% CO_2 at 37°C and growth medium was changed every 48 h until 70% confluence. The cells were then trypsinised, diluted 1:16 with growth medium and seeded in 8 ECM gel-coated 75 cm^2 CELLSTAR® filter cap cell culture flasks (passage 2). The growth medium was refreshed every 48 h.

When the cells reached 70% confluence, each flask was washed twice with PBS and incubated with 3 ml of 0.05% trypsin-EDTA (w/v) at 37°C for 3 min to dissociate the cells. 7 ml of growth medium was added to stop the protease activity. Cell suspension from the 8 flasks were pooled and centrifuged at 1,600 rpm for 5 min at room temperature. A freezing medium was prepared by adding 1 ml of DMSO (Sigma-Aldrich #D2650) to 9 ml of growth medium, which was then sterilised using a 0.2 μm Minisart syringe filter (Sartorius Stedim #16534, East Oakleigh, Victoria, Australia). The cell pellet was resuspended in 4 ml of growth medium, then 4 ml of FBS and 8 ml of freezing medium were added. The cell suspension was mixed quickly and divided into 1 ml

aliquots in Cryo.s™ Freezing Tubes (Greiner Bio-One #122278). The vials were frozen at -20°C for 30 min, followed by at -80°C overnight and stored in liquid nitrogen until use.

Prior to experiments, a vial of cells was rapidly thawed at 37°C and was then added to 9 ml of growth medium in a 15 ml conical tube (Greiner Bio-One #188261). The cells were centrifuged at 1,600 rpm for 5 min at room temperature. The cell pellet was resuspended in 2 ml of growth medium and the suspension transferred to an ECM gel-coated 75 cm^2 CELLSTAR® filter cap cell culture flask containing 8 ml of growth medium. The cells (passage 3) were maintained in an atmosphere of 5% CO_2 at 37°C. Growth medium was changed the next day and then every 48 h. The cells were passaged when they reached 70% confluence.

Experiments were performed on cells at passage 6. When cells at passage 5 reached 70% confluence they were trypsinised and diluted 1:10 with growth medium. Cells were seeded on ECM gel-coated culture plates and maintained in growth medium until 70% confluence. The growth medium was then replaced by the differentiation medium (α-MEM supplemented with 2% HS (v/v), 25 U/ml penicillin, 25 μg/ml streptomycin and 3 μg/ml amphotericin B). Experiments were conducted after 3 days of differentiation. Complete differentiation of cells into myotubes was confirmed visually as described in Section 2.2.1. Myotubes were rinsed twice with serum-free media (α-MEM supplemented with 0.1% BSA (w/v)) prior to treatments.

2.2.3 Total protein content of cell culture

Total protein content of each well or Petri dish was determined using the BCA™ Protein Assay Kit (Pierce #23225 distributed by Quantum Scientific, Murarrie, Queensland, Australia).

A set of protein standards (0 μg/ml, 5 μg/ml, 10 μg/ml, 25 μg/ml, 50 μg/ml, 100 μg/ml, 160 μg/ml and 250 μg/ml) was prepared by serial dilution of the Albumin Standard (BSA at 2 mg/ml in 0.9% saline (w/v) and 0.05% sodium azide (w/v); provided in the kit) with the lysis buffer used in the corresponding experiments. The assay was performed according to manufacturer's instructions. Standards and samples (25 μl; diluted based on pilot studies if necessary) were added to a 96-well plate (Sarstedt #82.1581.001, Newton, North Carolina, USA) in triplicates and 200 μl of working reagent (50:1 dilution of BCA™ Reagent A with BCA™ Reagent B) was added to each well. The plate was agitated for 30 sec at room temperature and then incubated at 60°C for 30 min, during which in the presence of an alkaline medium, Cu^{2+} was reduced to Cu^{+1} by the protein in the samples. A purple reaction product was then formed by the chelation of two molecules of bicinchoninic acid (BCA) with one Cu^{+1} ion. The plate was allowed to sit at room temperature for 20 min prior to absorbance measurement at 540 nm on a microplate reader (Bio-Tek Instruments #ELx808, Winooski, Vermont, USA). Total protein content of the cells was then determined using a 4-parameter curve with the software KC4 (version 3.3, Bio-Tek, Winooski, Vermont, USA).

2.3 Adipose tissue-conditioned medium

All solutions were warmed to 37°C before use unless specified and aseptic techniques in a biological safety cabinet were used for all procedures.

After removing visible connective tissues and blood vessels, the adipose tissue explant was immediately placed in ice-cold α-MEM and transported to the laboratory on ice. The sample was weighed, rinsed 3 times with ice-cold PBS and was then transferred to a Petri dish. The sample was cut into small pieces (~10 mg w.w.) and tissue fragments were incubated in 12-well plates (~ 80 mg w.w./well) containing α-MEM supplemented with 1% BSA (w/v), 25 U/ml penicillin, 25 μg/ml streptomycin and 3 μg/ml amphotericin B (1 ml/well) in an atmosphere of 5% CO_2 at 37°C. The medium was collected every 24 h and refreshed for 168 h. The medium collected, now referred to as adipose tissue conditioned-medium (CM), was sterilised using a 0.2 μm Minisart syringe filter and 1 ml aliquots were stored at -80°C until use.

2.4 Cell viability assays

2.4.1 Lactate dehydrogenase assay

Lactate dehydrogenase (LDH), a stable cytoplasmic enzyme present in all cells, is rapidly released into the cell culture supernatant when the plasma membrane is damaged. Since plasma membrane damage is a typical characteristic of cell death (Buja et al. 1993), an increase in dead or plasma membrane-damaged cells results in an increase of LDH activity in the culture supernatant and this makes the analysis of LDH release an accurate measure of plasma membrane integrity and cell viability in *in vitro* models irrespective of the type of cell death (Loo and Rillema 1998; Krysko et al. 2008). Measuring released LDH activity has previously been used to validate the integrity of tissue explants (Lappas et al. 2004) and the cytotoxicity of treatments on cell cultures (Peiro et al. 2001; Schultheiss et al. 2004).

LDH activity was measured using the Cytotoxicity Detection Kit^{PLUS} [LDH] (Roche Applied Science #04 744 926 001, Mannheim, Germany) and a standard curve (0 U/ml, 0.001 U/ml, 0.005 U/ml, 0.01 U/ml, 0.05 U/ml and 0.1 U/ml) was prepared by serial dilution of commercially available L-LDH (550 U/mg at 25°C; Roche Applied Science #10 127 876 001). The assay was performed according to manufacturer's instructions at room temperature. Standards, background control and samples (100 µl; diluted based on pilot studies if necessary) were added to a 96-well plate in triplicates and 100 µl of reaction mixture (1:45 dilution of reconstituted bottle 1 with bottle 2) was added to each well. The plate was agitated for 30 sec and then incubated for 30 min (protected from light). During the reaction lactate was converted to pyruvate by LDH and simultaneously NAD^+ was reduced to $NADH/H^+$. The H/H^+ from $NADH/H^+$ was then transferred to the yellow tetrazolium salt INT (2-[4-iodophenyl]-3-[4-nitrophenyl]-5-phenyltetrazolium chloride) which was reduced to the red formazan salt. After the incubation, 50 µl of Stop Solution was added to each well and the plate was agitated for 30 sec. Bubbles in the wells were removed prior to absorbance measurement at 490 nm using a microplate reader. LDH activity was determined using a 4-parameter curve with the software KC4. Released LDH activity was expressed as per volume of medium [U/ml] or protein content of cell culture [U/g].

2.4.2 Visualisation of DNA laddering

Internucleosomal DNA cleavage into oligonucleosome-length fragments is considered as the biochemical hallmark of cell death, which can be visualised on a gel as a distinct ladder of bands at multiples of ~ 180 base pairs (Wyllie 1980; Elmore 2007). The protocol to detect DNA laddering was adapted from methods described by Gullicksen et al (2004) and the modifications are detailed below.

2.4.2.1 Tissue homogenisation

Adipose tissue explants, 200 – 300 mg, were rinsed twice with ice-cold PBS, immediately frozen in dry ice and stored at -80°C until use. The sample was thawed to 4°C and was transferred to a 2 ml Tenbroeck Tissue Grinder (Wheaton Science #357422 distributed by Edwards Instruments, Narellan, New South Wales, Australia), in which the tissue was homogenised in 1 ml of lysis buffer (10 mM Trizma® hydrochloride (Tris-HCl, Sigma-Aldrich #T3253), 10 mM EDTA (Sigma-Aldrich #E1644) and 0.5% Triton® X-100 (Sigma-Aldrich #T8787; pH 8.0; v/v) for 30 sec. The homogenate was transferred to a 2 ml micro tube. The homogeniser was rinsed with 100 µl of lysis buffer which was then combined with the homogenate. The homogenate was incubated on ice for 20 min prior to centrifuge at 13,200 rpm for 15 min at 4°C. After removing the top fat layer, the supernatant was transferred to a new 2 ml micro tube. 1 ml of lysis buffer was added to the pellet and the centrifuge and collection of supernatant was repeated. The pellet (containing the insoluble DNA) and the pooled supernatant (containing the soluble DNA) were stored at -80°C until DNA extraction.

2.4.2.2 Extraction of DNA

The insoluble (intact) DNA was extracted using DNAzol (Molecular Research Center #DN127, Cincinnati, Ohio, USA) according to manufacturer's instructions and modified by Gullicksen et al (2004). DNAzol (0.5 ml) was added to the pellet, which was then dispersed by repeated pipetting. Ribonuclease (RNAse; Sigma-Aldrich #R6513) was added at a final concentration of 0.5 mg/ml, the samples were heated for 30 min at 37°C (protected from light), and then centrifuged at 13,200 rpm for 10 min at 4°C. The supernatant was transferred to a 2 ml micro tube and 3 µl of polyacyl carrier (Molecular Research Center #PC152) was added where after the solution was mixed by inversion.

DNA was precipitated by adding 250 µl of 100% ethanol (Sigma-Aldrich #E7023) followed by inverted mixing. The tube was allowed to sit for 3 min at room temperature, after which it was centrifuged at 13,200 rpm for 5 min at 4°C. The pellet was washed with 1 ml of 70% ethanol (absolute ethanol diluted with sterile 0.1% diethyl pyrocarbonate (DEPC; Sigma-Aldrich #D5758)-treated (v/v) deionised water; v/v) and mixed by inversion. The tube was allowed to sit for 5 min at room temperature and was then centrifuged at 7,000 rpm for 3 min at 4°C. Ethanol in the supernatant was discarded, followed by repeated washing. The DNA pellet was air-dried for 15 min and solublised in 75 µl of TE buffer (10 mM Tris-HCl and 1 mM EDTA; pH 8.0). The DNA was stored at -80°C until use.

Prior to the extraction of soluble (fragmented) DNA, the supernatant from homogenisation was thawed to 4°C and then treated with RNase at a final concentration of 0.5 mg/ml for 30 min at 37°C (protected from light). An equal volume of phenol/chloroform/isoamyl alcohol 25:24:1 (Sigma-Aldrich #P2069) was added. The solution was mixed by vortex for 15 sec and was then allowed to sit for 3 min at room temperature, followed by centrifugation at 13,200 rpm for 10 min at room temperature. The aqueous phase was transferred to a new 2 ml micro tube. TE buffer (100 µl) was added to the organic phase and the extraction of aqueous phase was repeated. The aqueous phase was pooled and an equal volume of phenol/chloroform/isoamyl alcohol was added. After centrifugation at 13,200 rpm for 3 min at room temperature, the aqueous phase was transferred to a 2 ml micro tube, and 8 µl of polyacyl carrier and magnesium chloride (Sigma-Aldrich #M8266; final concentration of 5 mM) and ½ volume of 7.5 M ammonium acetate (Sigma-Aldrich #A1542) was added to the supernatant and the solution was mixed by inversion. The DNA was precipitated by

adding an equal volume of isopropanol (Sigma-Aldrich #I9516). The solution was mixed and was kept for 30 min at -20°C. DNA was precipitated by centrifugation at 13,200 rpm for 30 min at 4°C and the pellet was washed with 1 ml 70% ethanol (v/v). The tube was allowed to sit for 5 min at room temperature prior to centrifugation at 7,000 rpm for 3 min at 4°C. The supernatant was discarded and the washing was repeated. The pellet was air-dried for 15 min, followed by solubilisation in 50 µl of TE buffer (pH 8.0). The sample was stored at -80°C until use.

Purity of both fractions of DNA was determined by ultraviolet (UV) spectrophotometry. The absorbance of the samples at 260 nm and 280 nm was measured by the Thermo Scientific NanoDrop™ 1000 (Thermo Fisher Scientific, Wilmington, Delaware, USA) against TE buffer (pH 8.0) as blank. A ratio of absorbance at 260 nm and 280 nm (A260/280) around 1.8 indicates DNA of good quality (Santella 2006).

2.4.2.3 Quantification of DNA

The concentration of double-stranded DNA (dsDNA) in both fractions was measured using the Quant-iT™ PicoGreen® dsDNA Assay Kit (Molecular Probes #P7589 distributed by Invitrogen, Mount Waverley, Victoria, Australia) according to manufacturer's instructions.

A DNA standard curve was prepared using the lambda DNA standard (100 µg/ml; provided in the kit). The standard was diluted 50-fold in TE buffer (pH 7.5; provided in the kit as 20x and was diluted with nuclease-free water (Ambion #AM9930 distributed by Applied Biosystems, Scoresby, Victoria, Australia) prior to use) to make a 2 µg/ml working solution, from which a DNA standard curve (0 ng/ml, 1 ng/ml, 10 ng/ml, 100

ng/ml and 1 µg/ml) was prepared by serial dilution with TE buffer (pH 7.5). Standards and samples (100 µl) were added to a 96-well plate in duplicates and 100 µl of the aqueous working solution of the Quant-iT™ PicoGreen® reagent (provided as 200x; diluted with TE buffer (pH 7.5) prior to use) was added to each of the wells. The plate was incubated for 5 min at room temperature (protected from light). After incubation, the fluorescence was measured using the microplate reader FLUOstar OPTIMA (BMG LABTECH, Mornington, Victoria, Australia) with standard fluorescein wavelengths (excitation 485 nm and emission 520 nm).

2.4.2.4 Agarose gel electrophoresis

A 2% agarose gel (w/v) was prepared by mixing 2 g of agarose (Promega #V3841, Sydney, New South Wales, Australia) with 100 ml of sterile 0.5x Tris-borate-EDTA (TBE) buffer (44.5 mM Trizma® base (Sigma-Aldrich #T1503), 44.5 mM boric acid (Sigma-Aldrich #B6768) and 1 mM EDTA; pH 8.3). The solution was heated in the microwave until the agarose was dissolved and the solution was clear, which was then allowed to cool to ~ 50°C under running water before pouring into a gel casting tray with a 20 wells comb. The gel was allowed to solidify for 20 min at room temperature. The comb was removed and the gel was transferred to the electrophoresis chamber, which was filled with ~ 800 ml of 0.5x TBE buffer.

Samples (27 µl) containing 45 ng of DNA (diluted with nuclease-free water if necessary) was mixed with 3 µl of 10x agarose gel loading buffer (60% glycerol (Sigma-Aldrich #G8773; v/v), 0.25% bromophenol blue (Sigma-Aldrich #114391; w/v) and 0.2 M EDTA; pH 8.3). SPP1/*Eco*RI DNA Molecular Weight Marker (8 µl; detection size 492 – 8,557 bp; GeneWorks #DMW-S1, Hindmarsh, South Australia, Australia) and

pUC19/*Hpa*II DNA Molecular Weight Marker (8 µl; detection size 34 – 501 bp; GeneWorks #DMW-P1, Hindmarsh, South Australia, Australia) were loaded on lanes 1 and 2 respectively. A 30 µl of aliquot of each sample (pre-mixed with loading buffer) were loaded on the rest of the wells. The gel was run at 120 V (8 V/cm) for 90 min.

2.4.2.5 Gel staining

The gel was stained with SYBR® Gold Nucleic Acid Gel Stain (Molecular Probes #S-11494) according to manufacturer's instructions and the procedures were completed at room temperature. The 10,000x stain concentrate was diluted with 0.5x TBE buffer (pH 8.0). The gel was fully immersed in the staining solution and was agitated for 40 min in the dark. The DNA ladder was visualised on an UV transilluminator (UVP #TFM-26, Upland, California, USA) and the image was photographed using the Kodak 1D image analysis software (version 3.5.3, Kodak, Rochester, New York, USA).

2.5 Cytokine profiling

2.5.1 Enzyme-linked immunosorbent assay (ELISA)

Leptin content in the CM was measured using a human leptin immunoassay kit (BioSource #KAC2281 distributed by Invitrogen, Mount Waverley, Victoria, Australia). Human Leptin Standard was reconstituted to 10,000 pg/ml with Standard Diluent Buffer. The solution was mixed gently and allowed to sit for 10 min at room temperature. A set of leptin standards (15.6 pg/ml, 31.2 pg/ml, 62.5 pg/ml, 125 pg/ml, 250 pg/ml, 500 pg/ml and 1,000 pg/ml) was prepared by serial dilution of the reconstituted standard with Standard Diluent Buffer. If necessary, CM was diluted with α-MEM supplemented with 1% BSA (w/v), 25 U/ml penicillin, 25 µg/ml streptomycin and 3 µg/ml amphotericin B.

The immunoassay was performed according to manufacturer's instructions and all procedures were completed at room temperature. Standard Diluent Buffer (100 µl) was added to the 'zero wells' of the plate, and 100 µl of standards, background control and samples were added to the appropriate wells of the plate in duplicates, followed by 100 µl of biotinylated anti-human leptin (Biotin Conjugate) to each well except the 'chromogen blanks'. The plate was tapped to mix and incubated for 2 h. After the incubation, the contents of the wells were aspirated and the wells were washed 4 times with 400 µl of Working Wash Buffer (1:25 dilution of the Wash Buffer Concentrate with deionised water). After the final wash, the contents of the wells were aspirated and the plate was tapped dry on paper towels. Streptavidin-HRP Working Solution (100 µl; 1:100 dilution of Streptavidin-HRP concentrate with Streptavidin-HRP Diluent) was added to each well except the 'chromogen blanks'. The plate was then incubated for 30 min, followed by washing as described above. After adding 100 µl of Stabilized Chromogen to each well, the plate was incubated in the dark for 30 min. Finally, 100 µl of Stop Solution was added to each well. The plate was tapped to mix and any bubbles in the wells were removed prior to absorbance measurement at 450 nm using an absorbance microplate reader. Leptin concentration in CM was determined using a 4-parameter curve with the software KC4 and was expressed as leptin released per tissue weight [ng/g w.w.].

2.5.2 Multiplex assay

The concentrations of adiponectin, IL-1β, IL-6, IL-8, TNF-α, resistin, PAI-1 (total) in CM were determined using a Human Adipocyte Linco*plex* Kit (Linco #HADCYT-61K distributed by Millipore, North Ryde, New South Wales, Australia). The Human Adipokine Standard Cocktail was reconstituted with 250 µl of deionised water and

allowed to sit for 5 min at room temperature. After vortex mixing, the standards were transferred to a micro tube and a set of standards was prepared by serial dilution using the Assay Buffer. CM at two concentrations, undiluted and 1:100, were used with α-MEM supplemented with 1% BSA (w/v), 25 U/ml penicillin, 25 μg/ml streptomycin and 3 μg/ml amphotericin B as diluent. Antibody-Immobilized Beads were prepared by adding 0.15 ml of each antibody bead to the Mixing Bottle and the final volume was brought to 3 ml with the Bead Diluent.

The assay was performed according to manufacturer's instructions and all procedures were completed at room temperature unless specified. The filter plate was blocked by adding 200 μl of Assay Buffer to each well. The plate was sealed and agitated on a plate shaker for 10 min. The Assay Buffer was then removed by vacuum and the bottom of the plate was dried using paper towels. Assay Buffer (25 μl) was added to the '0 standard' and sample wells. Standards, Controls (reconstituted prior with 250 μl of deionised water), adipokine-free media (α-MEM supplemented with 1% BSA (w/v), 25 U/ml penicillin, 25 μg/ml streptomycin and 3 μg/ml amphotericin B) and samples (25 μl) were added to the appropriate wells in duplicates. With intermittent mixing to avoid settling, 25 μl of the Mixed Beads was added to each well. The plate was sealed, covered with aluminium foil and incubated with agitation for 16 h at 4°C.

After the overnight incubation, the plate was allowed to warm to room temperature before removing the content by vacuum. The plate was washed 3 times by rinsing each well with 200 μl of Wash Buffer (1:10 dilution of the concentrate with deionised water) and removing the Wash Buffer with vacuum filtration between washes. The bottom of the plate was dried by paper towels after the final wash. Thereafter, 50 μl of Detection

Antibody Cocktail was added to each well. The plate was then sealed, covered with aluminium foil and incubated for 30 min with agitation followed by the addition of 50 µl of Streptavidin-Phycoerythrin to each well. Again, the plate was sealed, covered with aluminium foil and incubated on a plate shaker for 30 min. After removing the content by vacuum, the plate was washed as described above. Finally, 100 µl of Sheath Fluid (1:20 dilution of the concentrate with type II water; Bio-Rad #171-000055, Gladesville, New South Wales, Australia) was added to all wells. The beans were resuspended by agitating the sealed and aluminium foil-covered plate for 5 min.

Multianalyte profiling was performed on the LiquiChip 200 Workstation (Qiagen #9001382, Melbourne, Victoria, Australia) and fluorescence data were analysed by using the LiquiChip Analyzer Software (version 1.0.5, Qiagen, Melbourne, Victoria, Australia). The concentrations of the cytokines were expressed per tissue weight [ng/g w.w. or pg/g w.w.].

2.6 Fatty acid profiling

Fatty acid profile in CM was measured using gas chromatography. Lipids were extracted according to the method described by Folch et al (1957). Fatty acids were methylated and fatty acid methyl esters (FAMEs) were extracted and purified as described by Christie (1989). Internal standard solution was prepared by adding 13.22 mg triheptadecanoin (Sigma-Aldrich #T2151) to 25 ml chloroform to give a final concentration of triglyceride (17:0) of 0.5 mg/ml. Sulphuric acid (1%; Sigma-Aldrich #320501; v/v) in dry methanol was prepared by refluxing over calcium hydride (Sigma-Aldrich #213268) for 1 h followed by distillation.

Internal standard solution (50 µl), 800 µl of sample, 1.35 ml of methanol and 2.7 ml of chloroform were added to a 125 mm x 16 mm cell culture tube (BD #353033, North Ryde, New South Wales, Australia). The solution was mixed vigorously for 30 sec. HCl (10 µl; 5 M; Sigma-Aldrich #H1758) was added and the solution was mixed vigorously for 30 sec and centrifuged at 2,000 rpm for 10 min at room temperature. After removing the aqueous phase by aspiration, the lower organic layer was transferred to a cell culture tube and evaporated under nitrogen to dryness at 40°C. The fatty acids were methylated in 1.5 ml of 1% sulphuric acid in dry methanol (v/v) and the solution was heated for 18 h at 50°C. After cooling to room temperature, FAMEs were extracted by adding 3 ml of glass-distilled water and 5 ml of petroleum spirit (boiling range 40 – 60°C; Merck #10178.4F, Kilsyth, Victoria, Australia) and the solution was mixed vigorously for 30 sec. The organic phase was transferred to a cell culture tube and the extraction was repeated, followed by evaporation to dryness under a stream of dry nitrogen. The FAMEs were dissolved in 1.5 ml of hexane (Sigma-Aldrich #32293) and cleaned on 20 mm florisil columns (Sigma-Aldrich #F7752) with an additional 1 ml of hexane. The FAMEs were then eluted with 2 ml of 10% diethyl ether (Sigma-Aldrich #31671; v/v) in hexane and the eluate was collected in conical vials, dried under nitrogen, and then the purified FAMEs were dissolved in 30 µl of isooctane (Sigma-Aldrich #59030). FAMEs were separated using an Agilent 6890 gas chromatograph (Agilent Technologies, Biolab, Scoresby, Victoria, Australia). A 0.2 µl aliquot of FAMEs was injected onto a BPX70 capillary column (30 m x 0.53 mm x 0.5 µm film thickness; SGE International, Sydney, New South Wales, Australia) using hydrogen as the carrier gas. Peak identification was based on a comparison of retention times with a standard mix (Supelco® 37 Component FAME mix; Sigma-Aldrich #47885-U). Peak areas were measured using the DELTA Chromatography Data Systems (version 5.0, DataworX Pty Ltd, Brisbane, Queensland,

Australia). Peak areas were then converted to absolute values based on the area of the internal standard peak and its known concentration in the samples. The concentrations of the fatty acids were expressed per tissue weight [mmol/g w.w.].

2.7 Glucose uptake in skeletal muscle cells

The protocol for glucose uptake assay was modified from that described by Ciaraldi et al (1995). Uptake buffer, which consisted of 150 mM sodium chloride (Sigma-Aldrich #S6191), 5 mM potassium chloride (Sigma-Aldrich #P5405), 1.2 mM magnesium sulfate heptahydrate (Sigma-Aldrich #M2773), 2.5 mM sodium phosphate monobasic (Sigma-Aldrich #S3139), 1.2 mM calcium chloride dihydrate (Sigma-Aldrich #C5080), 10 mM 4-(2-Hydroxyethyl)piperazine-1-ethanesulfonic acid (HEPES; Sigma-Aldrich #H4034) and 0.1% BSA (w/v) was prepared the day prior to experiment and was kept at 4°C until use.

Skeletal muscle cells were cultured on 12-well plates and each experimental condition run in triplicate, and at the completion of each the content of the plate was aspirated. After rinsing 3 times with the uptake buffer, 1 ml of uptake buffer was added to each well. The glucose uptake assay was started by adding 11 µl of 1 mM 2-deoxy-D-glucose (Sigma-Aldrich #D8375; made up in sterile deionised water and stored at 4°C prior to use), pre-mixed with 2-[^{3}H(N)]-deoxy-D-glucose (specific activity: 8 Ci/mM, 1 mCi; Perkin Elmer #NET328A001MC, Melbourne, Victoria, Australia) in a ratio of 1:10, to each well to give the final concentrations of 2-deoxy-D-glucose and 2-[^{3}H(N)]-deoxy-D-glucose at 10 µM and 1 µCi/well respectively. A triplicate of blanks was prepared by culturing the cells under control conditions and with only 2-deoxy-D-glucose added during the glucose uptake assay. A space out of 20 sec was allowed between additions of

the 11 µl of 2-deoxy-D-glucose mix to each well. After 15 min incubation at 37°C, the reaction buffer was aspirated and ~ 2 ml of ice-cold PBS was added to stop the reaction with 20 sec space out between wells until all reactions were stopped. Each well was then rinsed repeatedly with ice-cold PBS for a total of 4 washes. After the PBS was aspirated, 0.5 ml of 0.1 M sodium hydroxide (NaOH; Sigma-Aldrich #S8045; made up with sterile deionised water prior to use) was added to each well. The cells were allowed to solubilise in NaOH for 30 min at room temperature, after which 0.4 ml of cell lysate from each well was transferred to scintillation vials (Crown Scientific #933, Minto, New South Wales, Australia) containing 4 ml of Ultima Gold™ (Perkin Elmer #6013329), a liquid scintillation cocktail, for the determination of cell-associated radioactivity using the Liquid Scintillation System (Beckman Coulter #LS6000LL, Fullerton, California, USA). The samples were counted 3 times and the average of the counts was used in subsequent analysis. The rest of the lysate was collected and stored at -80°C until the determination of protein content as described in Section 2.2.3. Glucose uptake is expressed as picomoles of 2-deoxy-D-glucose taken up per min per mg of total protein.

2.8 Quantification of gene expression

2.8.1 mRNA quantification via 'Real Time' Polymerase Chain-Reaction (RT-PCR)

2.8.1.1 RNA extraction

Skeletal muscle cells were cultured on 6-well plates. After treatment, the content of the plate was aspirated and each well was washed twice with 2 ml of ice-cold PBS. Keeping the plate on ice, 800 µl of Trizol® Reagent (Invitrogen #15596-018) was added to each well and the plate was gently agitated. The cell lysate was passed through the pipette for several times, which was then collected and stored in PCR-clean micro tubes at -80°C until RNA extraction.

The protocol for RNA extraction was modified from manufacturer's instructions. All micro tubes were PCR-clean and all centrifugation was performed at 4°C. Chloroform (200 µl; Sigma-Aldrich #366927) was added to the cell lysate. The tube was inverted to mix for 15 sec and allowed to sit on ice for 5 min. The cell lysate was then centrifuged at 13,200 rpm for 15 min and the aqueous phase was transferred to a fresh micro tube. RNA was precipitated by adding isopropanol (~ 80% of the volume of the aqueous phase) and 10 µl of 5 M sodium chloride. The content of the tube was mixed by inversion and the tube was kept for 3 h at -20°C, which was then centrifuged at 13,200 rpm for 20 min. After centrifugation, the RNA was precipitated to form a pellet on the bottom of the tube and the supernatant was aspirated. The RNA pellet was washed by adding 800 µl of 75% ethanol (absolute ethanol diluted with sterile 0.1% DEPC-treated (v/v) deionised water; v/v), followed by centrifugation at 9,000 rpm for 8 min. The ethanol was aspirated and the RNA pellet was air-dried for 5 min. Finally, the RNA pellet was dissolved in 5 µl of nuclease-free water (heated to 60°C prior to use) and the RNA solution was mixed thoroughly. The RNA was stored at -80°C until use.

2.8.1.2 Determination of purity and quantity of RNA

The purity and quantity of RNA was determined by absorbance of the samples at 260 nm and 280 nm and measured by the Thermo Scientific NanoDrop™ 1000 against nuclear-free water as blank. Samples with an A260/280 ratio of 1.9 – 2.1 was considered as pure RNA or relatively free from contaminants (Santella 2006). RNA yield was also quantified by the same analysis system using the reading of absorbance at 260 nm equivalent to 40 µg/ml of single-stranded RNA, which was calculated and expressed as [ng/µl].

2.8.1.3 Reverse transcription of RNA

RNA was reverse-transcribed to cDNA using the QuantiTect Reverse Transcription Kit (Qiagen #205311) according to manufacturer's instructions and all procedures were completed on ice unless specified. A 0.5 µg aliquot of RNA was added to 0.2 ml PCR tubes (Eppendorf # 0030 124.359 distributed by Crown Scientific) and the final volume was brought to 6 µl with nuclease-free water. A 'No RT' control was set up without the presence of RNA to detect genomic DNA contamination in the subsequent RT-PCR reaction. gDNA Wipeout Buffer (1 µl) was added to each tube. The tubes were mixed and incubated for 2 min at 42°C in the Mastercycle® gradient (Eppendorf #5331 000.010) and then were placed immediately on ice. The reverse-transcription reaction master mix was prepared by mixing 0.5 µl of Quantiscript Reverse Transcriptase, 2 µl of Quantiscript RT Buffer and 0.5 µl of RT Primer Mix for each reaction. Master mix (3 µl) was added to the template RNA. The tubes were then incubated in the Mastercycle® gradient using the following setting: 42°C for 30 min, 95°C for 3 min and 4°C for 10 min. cDNA was then stored at -20°C until use.

2.8.1.4 Primer preparation

Primers for cyclophilin B, AMPKα2, SPTLC1 and SCD1 were purchased from Qiagen (QuantiTect Primer Assay; Qiagen, Doncaster, Victoria, Australia). The primers were reconstituted with 1.1 ml of nuclease-free water according to manufacturer's instructions. After mixing by vortex, 200 µl aliquots of the reconstituted primer (10x stock) were stored at -20°C until use.

Primers for AMPKα1, PDK4, PGC-1α, LKB1 and SPTLC2 were purchased from GeneWorks (Hindmarsh, South Australia, Australia). Primer sequences for AMPKα1

(Fukuyama et al. 2007), PDK4 (McAinch et al. 2003) and PGC-1α (McAinch et al. 2003) are published elsewhere. Primers for LKB1 and SPTLC2 were designed using the Primer Express software package (version 1.0, Applied Biosystems, Foster City, California, USA) from gene sequences obtained from GenBank (LKB1 – NM_001108069; SPTLC2 – NM_001037097). Forward and reverse primer sequences are shown in Table 2.1. The primers were reconstituted to 100 μM according to manufacturer's instructions. The volume of nuclease-free water added was calculated using the following formula: volume of water added [μl] = (weight of primer per tube [μg] / molecular weight) x 10,000. The reconstituted primer was stored at -20°C until use. The optimal working concentrations of primers from GeneWorks and cDNA for the RT-PCR reaction (i.e., threshold cycle (C_T) values fall between 15 and 30) were determined in pilot studies.

Table 2.1 Primer sequences.

Gene[1]	Forward Primer	Reverse Primer
AMPKα1	TGTGACAAGCACATTTTCCAA	CCGATCTCTGTGGAGTAGCAG
PDK4	GGGATCTCGCCTGGCACTTT	CACACATTCACGAAGCAGCA
PGC-1α	ACCCACAGGATCAGAACAAACC	GACAAATGCTCTTTGCTTTATTGC
LKB1	CCTACTCCGAGGGATGTTGGA	GGAACCAGCTGTGCTGTCTAATC
SPTLC2	GAGGCAAGAAGGAGCTGATAGACT	TGACATCGACGTGGCATACA

[1] Accession: AMPKα1 – NM_019142; PDK4 – NM_053551; PGC-1α – NM_031347; LKB1 – NM_001108069; SPTLC2 – NM_001037097

2.8.1.5 RT-PCR

mRNA expression was determined by RT-PCR using the QuantiTect SYBR Green PCR Kit (Qiagen #204143). The RT-PCR reaction was performed according to manufacturer's instructions. All procedures were completed on ice unless specified. For each reaction, a master mix was prepared by mixing 6 µl of nuclease-free water, 2 µl of primers and 10 µl of QuantiTect SYBR Green PCR Master Mix. Master mix (18µl) was added to each 0.1 ml strip tubes (Corbett Research #3001-002, distributed by Adelab Scientific, Thebarton, South Australia, Australia). 2 µl of cDNA template and 'No RT' control was added to the corresponding tubes in triplicates and duplicates respectively. 'No Template' control was set up by adding 2 µl of nuclease-free water to 18 µl of master mix to detect contamination of reagents. The tubes were then placed in the LightCycler (Corbett Research #RG-3000) and the cycling program was started with the program detailed in Table 2.2.

Table 2.2. Real-Time PCR conditions.

Step	Time	Temperature	Ramp
PCR initial activation	15 min	95°C	20°C/sec
Cycling			
- Denaturation	15 sec	94°C	20°C/sec
- Annealing	30 sec	55°C	20°C/sec
- Extension	30 sec	72°C	2°C/sec
Cycle number	40 cycles		

The fluorescence data were analysed using the Rotor-Gene 6 Software (version 6.0, Corbett Research, Concorde, New South Wales, Australia). C_T was determined in each sample, which was the cycle in which the first increase in fluorescence was detected. A melting curve analysis was performed to verify the specificity of PCR products.

A standard curve for each target gene was constructed by plotting C_T against the log of dilutions of its PCR products (1/8 million, 1/80 million, 1/800 million, 1/12 billion and 1/16 billion). C_T of the experimental samples was then used to determine the relative abundance of starting templates.

2.8.2 Gene expression profiling via microarray analysis

2.8.2.1 RNA extraction

Extraction of RNA for microarray analysis was performed using the Aurum™ Total RNA Mini Kit (Bio-Rad #732-6820) according to manufacturer's instructions. The lysis solution was reconstituted with 500 µl of β-mercaptoethanol (Bio-Rad #161-0710). The low stringency wash solution concentrate (5x) was diluted with 80 ml of absolute ethanol (Sigma-Aldrich #E7023). DNase I was reconstituted by adding 250 µl of 10 mM Tris-HCl (pH 7.5) and stored at -20°C until use. All centrifugation steps were performed at 13,200 rpm at room temperature.

Skeletal muscle cells were cultured on 6-well plates. The treatment was stopped by aspirating contents of the wells. Each well was rinsed twice with 2 ml of ice-cold PBS. Keeping the plate on ice, 350 µl of lysis solution was added to each well. Cells were scrapped from the bottom of the wells using a disposable cell scrapper (Greiner Bio-One #541070). The cell lysate was passed through a 29G 1 ml insulin syringe (Terumo #U-

100) for 5 times to lyse cells thoroughly, and 350 µl of 70% ethanol (absolute ethanol diluted with sterile 0.1% DEPC-treated (v/v) deionised water; v/v) was added to each tube and mixed thoroughly until no bilayer was visible and viscosity was minimal. The homogenised lysate was then transferred to an RNA binding column and was centrifuged for 30 sec, after which the filtrate was discarded, and 700 µl of reconstituted low stringency wash solution was added to the column, centrifuged for 30 sec, and the filtrate removed. Diluted DNase I (80 µl; prepared prior by mixing 5 µl of reconstituted DNase I and 75 µl of DNase dilution solution) was added onto the centre of the membrane stack at the bottom of the column. The column was allowed to sit for 15 min at room temperature and was centrifuged for 30 sec with the digest buffer discarded afterwards. Thereafter, 700 µl of high stringency wash solution was added to the column. The tube was centrifuged for 30 sec and the wash solution was discarded. Finally, 700 µl of reconstituted low stringency wash solution was added to the column. The column was centrifuged for 1 min, and after discarding the wash solution the column was centrifuged for an additional 2 min to remove any residual wash solution.

The column was transferred to a 1.5 ml PCR-clean micro tube and 30 µl of elution solution (warmed to 70°C prior to use) was added onto the centre of the membrane stack at the bottom of the column. The membranes were allowed to saturate with the solution for 1 min. The column was centrifuged for 2 min to elute the total RNA, which was then stored at -80°C until use.

2.8.2.2 Sample validation

The quantity and purity of RNA was determined by UV spectrophotometry using the Thermo Scientific NanoDrop™ 1000 as described in section 2.8.1.2 against elution solution as blank.

The integrity of RNA was determined by agarose gel electrophoresis. A 1.5% gel (w/v) was prepared by adding 1.5 g agarose to 100 ml of sterile 0.5x TBE buffer (pH 8.3) with 1 mg/ml of ethidium bromide (Sigma-Aldrich #E1510). The gel was then prepared as described in section 2.4.2.4. The solidified gel was transferred to the electrophoresis chamber, which was filled with ~ 800 ml of 0.5x TBE buffer with 1 mg/ml ethidium bromide. A 2 µl aliquot of 10x agarose gel loading buffer (pH 8.3) was mixed with 12 µl of samples containing 300 ng of RNA (diluted with nuclease-free water if necessary). In lane 1, 6 µl of SPP1/*Eco*RI DNA Molecular Weight Marker (detection size 492 – 8,557bp) was loaded and 14 µl of samples (mixed prior with loading buffer) were loaded on the rest of the wells. The gel was run at 120 V (8 V/cm) for 45 min. The gel was visualised and the image photographed as described in Section 2.4.2.5. A ratio of 28 S (~ 5 kb) to 18 S (~ 2 kb) ribosomal RNA of 2.0 and higher was considered an indicator of RNA of high quality (Schroeder et al. 2006).

The effect of treatment on mRNA expression of target genes were verified with results from previous studies (Section 6.3.1) by reverse transcription of RNA (Section 2.8.1.3) followed by RT-PCR (Section 2.8.1.4).

2.8.2.3 Gene expression profiling

RNA (300 ng), at a concentration of 100 ng/µl or higher from each replicate, was sent to the Adelaide Microarray Centre (Adelaide, South Australia, Australia) for RNA integrity assessment and Whole-Transcript Expression Analysis.

The assessment of RNA integrity of samples was performed on the Agilent 2100 Bioanalyzer (Agilent Technologies #G2940CA, Forest Hill, Victoria, Australia) using the Agilent RNA 6000 Nano Kit (Agilent Technologies #5067-1511) according to manufacturer's instructions. The data were analysed using the 2100 Expert Software (version B.02.06.S1418, Agilent Technologies) and expressed as RNA Integrity Number (RIN).

The Whole-Transcript Expression Analysis was performed by hybridising RNA to the GeneChip® Rat Gene 1.0 ST Array (Affymetrix, distributed by Millennium Science, Surrey Hills, Victoria, Australia) according to manufacturer's instructions. Each of the 27,342 genes was represented by ~ 26 probes spread across the full length of the gene. Array washing and staining were performed on the GeneChip® Fluidics Station 450 (Affymetrix #00-0079). The chip was then scanned using the GeneChip® Scanner 3000 7G (Affymetrix #00-0210) and hybridisation images were produced and analysed to obtain an intensity value for each probe using the Partek Genomics Suite (version 6.4, Partek, St. Louis, Missouri, USA) and the Limma package for Windows (version 2.14.6, Bioconductor, Seattle, Washington, USA). Principal Components Analysis (PCA) was used to visualise and summarise the dataset in respect to different experimental conditions (Raychaudhuri et al. 2000).

2.8.2.4 Data processing

Intensity-dependent ratio of raw microarray data were visualised using the *M* versus *A* (MA)-plot, where *M* is the intensity log-ratio (i.e., $M = \log_2 R - \log_2 G$) and *A* as the mean log intensity (i.e., $A = (\log_2 R + \log_2 G)/2$) where *R* and *G* were the background-corrected red and green intensities for each spot (Smyth and Speed 2003). Raw microarray data were also transformed into log intensity to visualise variation within the array using a basic box-plot. The raw intensity values were background-corrected, quantile-normalised and log (base 2)-transformed at the probe level using the Robust Multi-array Average (RMA). A linear model was then fitted to the normalised data to obtain an expression measure for each probe set on the array (Irizarry et al. 2003). Bayesian statistics as implemented in R and Bioconductor (Bioconductor, Seattle, Washington, USA), an open source platform and open development software project for the analysis and comprehension of genomic data, were used to define genes regulated (convergent/divergent) by each treatment using a log fold-change cut-off of 1.5 and/or Benjamini & Hochberg (BH) adjusted p-value of < 0.01 (Benjamini and Hochberg 1995).

Once the amount of repression and induction for each gene in response to each experimental condition was determined, the data were clustered hierarchically using MADE4 (version 1.2.0, Bioconductor, Seattle, Washington, USA), an R package for multivariate analysis of microarray data (Culhane et al. 2005). Samples with similar gene expression profiles, as determined by correlation value, were grouped together in a dendrogram. Samples showing few differences in gene expression levels may not cluster according to their biological category and thus may be identified as outliers. In addition, genes with similar expression patterns in response to specific experimental conditions

were also grouped in hierarchical clustering which helped identify gene product interactions and functional pathways.

Pathway analysis was performed to identify consistent changes in the expression of genes with related functions by integrating the normalised dataset and their functional annotations using the Gene Ontology (GO) (Ashburner et al. 2000; Curtis et al. 2005). Pathway enrichment for experimental condition was scored based on a significant shift in the hypergeometric distribution of genes regulated in each of the annotated GO categories. Categories exhibiting enrichment due to array constituent bias were excluded.

2.9 Fluorescent Western blotting

2.9.1 Protein extraction from L6 cells

All procedures were completed on ice and centrifugation at 4°C unless specified. As shown in Table 2.3, 1 ml aliquots of lysis buffer were prepared 3 h prior to protein extraction and were kept on ice until use (Hardie et al. 2000).

Table 2.3. Preparation of lysis buffer (1ml aliquot).

Order to add	Chemical	Volume to added [µl]
1	Deionised water	163.8
2	Mixture of:	
	- 500 mM Tris-HCl	
	- 10 mM EDTA	
	- 10 mM EGTA (Sigma-Aldrich #E4378)	
	- 500 mM NaF (Sigma-Aldrich #201154)	
	- 50 mM NaPPi (Sigma-Aldrich #S9515)	500
3	Glycerol	100
4	Triton X-100	10
5	1 mg/ml SBTI (Sigma-Aldrich #T9003)	10
6	1 mg/ml Leupeptin (GE Healthcare #US18413)	5
7	5 mg/ml Aprotinin (GE Healthcare #US11388)	7.8
8	1 mg/ml Pepstatin A (GE Healthcare #US20037)	3.4
9	10 mM DL-Dithiothreitol (Sigma-Aldrich #D9163)	100
10	10 mM PMSF (Sigma-Aldrich #P7626)	
	(added immediately before use)	100

Abbreviations: EDTA – Ethylenediaminetetraacetic acid disodium salt dihydrate, EGTA – Ethylene glycol-bis (2-aminoethylether) –*N,N,N',N'*-tetraacetic acid; NaF – Sodium fluoride; NaPPi – Sodium pyrophosphate tetrabasic decahydrate; SBTI – Soybean trypsin inhibitor; PMSF – Phenylmethylsulfonyl fluoride

Skeletal muscle cells were cultured on Petri dishes and were treated in duplicates. To harvest the cells, the dish was kept on ice and the culture medium was aspirated. The cells were rinsed twice with ice-cold PBS and 150 µl of lysis buffer was added and the cells were scrapped using a disposable cell scrapper. Cell lysates of the duplicates were combined in a 1.5 ml micro tube, which was then centrifuged at 13,200 rpm for 4 min. The supernatant was collected, with 30 µl transferred to a 0.5 ml micro tube for the determination of protein content as described in Section 2.2.3 and the remainder divided into 4 aliquots (~ 70 µl each) for western blot measurements. All supernatant were stored at -80°C until use.

2.9.2 NuPAGE® electrophoresis system

2.9.2.1 Preparation of samples

All procedures were performed on ice unless specified. Protein (81.7 µg) was diluted with deionised water to a total volume of 70 µl. NuPAGE® LDS Sample Buffer (17.5 µl; 4x; Invitrogen # NP0007) and NuPAGE® Reducing Agent (7 µl; 10x; Invitrogen # NP0004) were added to the samples. The samples were heated for 5 min at 95°C and then cooled on ice for 5 min, followed by centrifugation at 3,000 rpm for 5 min. The samples were kept on ice until loading on gels.

2.9.2.2 Electrophoresis of NuPAGE® Gels

The 1.5 mm x 10 well NuPAGE® Novex Tris-Acetate Gels (Invitrogen # EA0378BOX) were rinsed with deionised water. The tape and the comb were removed from the cassettes. The sample wells were rinsed 3 times with running buffer (prepared prior by a 1:20 dilution of Novex® Tris-Acetate SDS Running Buffer (20x; Invitrogen # LA0041) with deionised water) and were filled with running buffer after the final wash.

Two gels were inserted into the XCell *SureLock*™ Mini-Cell (Invitrogen #EI0001) and were locked in place with the Gel Tension Lodge. The second gel cassette was replaced by a plastic Buffer Dam when one gel was used. The Upper Buffer Chamber was filled with ~ 200 ml of running buffer until the level exceeded that of the wells. NuPAGE® Antioxidant (0.5ml; Invitrogen # NP0005) was added to the Upper Buffer Chamber. Full-Range Rainbow Molecular Weight Markers (15 µl; Amersham #RPN800 distributed by GE Healthcare, Piscataway, New Jersey, USA), AMPK Control Cell Extracts (10 µl; positive control; Cell Signaling #9158 distributed by Genesearch, Arundel, Queensland, Australia) and samples (30 µl; 35 µg of protein per lane) were loaded onto the gels. The Lower Buffer Chamber was filled with ~ 600 ml of running buffer until the chamber was completely full. The gels were run at 150 V for 1.25 h or until the electrophoresis was complete.

2.9.2.3 Western transfer using the XCell II ™ Blot Module

Transfer buffer was prepared by mixing 50 ml of NuPAGE® Transfer Buffer (20x; Invitrogen # NP0006), 200 ml of methanol (Sigma-Aldrich #270474) and 750 ml of deionised water. After soaking in transfer buffer, two blotting pads (Invitrogen #EI9052) were transferred to the gel/blot assembly tray (Criterion Blotter with Plate Electrodes; Bio-Rad # 170-4070). A PVDF membrane (Invitrolon™ PVDF/Filter Paper Sandwiches; Invitrogen #LC2005) was pre-wet in methanol for 30 sec. After a brief rinse with deionised water, the membrane was soaked in transfer buffer for several minutes.

Immediately following electrophoresis, the gel cassette was separated using the Gel Knife (Invitrogen #EI9010) and the gel was allowed to remain on one of the plates. The wells and the bottom lip of the gel were removed. A piece of filter paper was briefly

soaked in transfer buffer and was placed on top of the gel. Air bubbles trapped between the filter paper and the gel were removed. The plate was turned over (with the filter paper facing downwards) and placed on blotting pads already in the assembly tray. The cassette plate was removed after the filter paper and the gel were positioned on the blotting pads. Any trapped air bubbles were removed. A pre-soaked membrane, followed by a pre-soaked filter paper, was placed on the gel and air bubbles were removed. Finally, two soaked blotting pads were placed on the filter paper to complete the gel/membrane/filter paper assembly as shown in Figure 2.1A. When two gels were transferred, the gel/membrane/filter paper sandwich was assembled as shown in Figure 2.1B.

Figure 2.1. Gel/membrane/filter paper assembly when transferring one (A) or two (B) gels. Adapted from the NuPAGE® Technical Guide: General information and protocols for using the NuPAGE® electrophoresis system, version E, October 1, 2003, IM-1001, Invitrogen.

After all air bubbles were removed, the gel/membrane/filter paper assembly was transferred to the cathode (-) core of the XCell II™ Blot Module (Invitrogen # EI9051) with the assembly fitted horizontally across the bottom of the module. The anode (+) core was placed on the top of the pads so that the gel/membrane/filter paper assembly was held securely between the two halves of the blot module. The blot module was put in the Lower Buffer Chamber and locked in position by the Gel Tension Wedge. The module and the Outer Buffer Chamber were filled with transfer buffer and deionised water respectively. After adding 0.2 ml of NuPAGE® Antioxidant to the blot module, the transfer was run at 30 V for 2 h.

2.9.3 Reversible membrane staining

Ponceau S dye was used for reversible staining of protein bands on PVDF membranes. 0.1% Ponceau S (Sigma-Aldrich #P3504; w/v) was prepared in 5% acetic acid (Sigma-Aldrich #45726; v/v) and stored at room temperature. A stock of 10x Tris-buffered saline (TBS; 24.2 g of Trizma® base (Sigma-Aldrich #T1503) and 80 g of sodium chloride in 1 L of deionised water; pH 7.6) was prepared for subsequent washing which used 1x TBS (1:10 dilution of 10x TBS in deionised water). All staining and washing steps were performed at room temperature with agitation.

After transfer, protein bands on the membrane were temporarily stained by 25 ml of 0.1% Ponceau S in square Petri dish (Sarstedt #82.9923.422) for 5 min. Excess stain was removed by washing the membrane in deionised water for another 5 min. The weight bands of protein markers were marked and the stain was removed by washing the membrane with 25 ml of 1x TBS for 5 min.

2.9.4 Western blotting

Blocking buffer (1xTBS with 0.1% Tween® 20 (Sigma-Aldrich #P9416; v/v) and 5% ECL Blocking Agent (Amersham #RPN2125; w/v)) and wash buffer (1x TBS with 0.1% Tween® 20; v/v) were made fresh for each blot. All incubation and washing steps were performed at room temperature with agitation unless specified. Secondary antibody (Sheep anti-Rabbit IgG, Alkaline Phosphatase conjugate; Millipore #AP304A) was reconstituted with 1 ml of sterile deionised water and 1 ml of glycerol and stored at 4°C until use.

Membranes were incubated in 10 ml of blocking buffer for 70 min, followed by 3 washes with 25 ml of wash buffer (10 min, 10 min and 5 min) with deionised water rinsing between washes. Membranes were cut into strips to allow the detection of multiple proteins, which were then incubated in 3.5 ml of primary antibody against the target protein (Table 2.4) at 4°C and then at room temperature for 16 h and 1 h respectively, followed by repeated washing with 25 ml of wash buffer (10 min, 10 min and 5 min) as described above. Membranes were then incubated in 3.5 ml of reconstituted secondary antibody at a dilution of 1:5,000 in 1x TBS with 0.05% Tween® 20 (v/v) and 5% ECL Blocking Agent (w/v) for 1 h. Finally, the membranes were washed 3 times with 25 ml of wash buffer (10 min, 10 min and 5 min) and were soaked in 1x TBS prior to fluorescence detection.

Table 2.4. Primary antibody preparation.

Antibody[2]	Concentration	Dilution Buffer
β-actin (13E5)	1:25,000	1xTBS/0.1% Tween-20 with 5% BSA
AMPKα	1:1,000	1xTBS/0.1% Tween-20 with 5% BSA
Phospho-AMPKα (Thr172)	1:1,000	1xTBS/0.1% Tween-20
ACC	1:1,000	1xTBS/0.1% Tween-20 with 5% BSA
Phospho-ACC (Ser79)	1:1,000	1xTBS/0.1% Tween-20

[2] Antibodies were purchased from Cell Signaling (Danvers, Massachusetts, USA): β-actin – #4970; AMPKα – #2532; phosphor-AMPKα (Thr172) – #2532; acetyl-CoA carboxylase (ACC) – #3662; phosphor-ACC (Ser79) – #3661

2.9.5 Chemifluorescence detection

ECF™ Substrate (GE Healthcare #RPN5785) was reconstituted with 60 ml of dilution buffer according to manufacturer's instructions. Aliquots were stored at -20°C until use. Fluorescence was scanned using the imager Typhoon Trio™ (Amersham Biosciences #63-0055-87 distributed by GE Healthcare) and detected using the software Typhoon™ Scanner Control (version 5.0, Amersham Biosciences, Piscataway, New Jersey, USA).

The reconstituted ECF™ Substrate was applied on a glass surface at 5 μl/cm^2 of blot. After draining the excess 1x TBS, the blot (protein-side down) was placed on the ECF™ Substrate (with the blot completely covered with ECF™ Substrate) and incubated at room temperature. The incubation duration depended on the concentration of the target protein on the blot and was determined for each new Western application. The excess reagent was drained and the developed blot (protein-side down) was placed onto the glass platen of Typhoon™ with trapped air bubbles removed. The following parameters and PMT voltage setting were used for imaging chemifluorescent Western blots: Sensitivity – Normal; PMT – 800 V; Excitation – 532 nm; Emission filter – 526 SP.

The acquired image was analysed using an image analysis software package ImageQuant (version 5.2, Molecular Dynamics, Sunnyvale, California, USA). Integrated fluorescent signal was quantified using object one-dimensional (1-D) blot analysis, in which bands were identified manually and enclosed by boxes. All image pixels, also referred to as volume, bounded by each box were used for signal quantification. A value of integrated signal was generated by volume analysis within the box surrounding each separate band. All signals were normalised to a background value which was selected from a different region of the same membrane.

2.10 Data analysis

Data are expressed as means ± standard error of mean (SEM). Statistical analyses were performed by Student's *t* test, one-way or two-way analysis of variance (ANOVA) with Bonferroni post hoc tests to compare treatment difference using the GraphPad Prism Program (Version 5.01, GraphPad Software Inc., San Diego, California, USA) and SPSS (Version 12.0 for Windows, SPSS Inc., Chicago, Illinois, USA). Significance was accepted at $P < 0.05$.